AMERICAN JOURNAL OF PHYSICAL ANTHROPOLOGY 151:372–397 (2013)

A Calcaneus Attributable to the Primitive Late Eocene Anthropoid *Proteopithecus sylviae*: Phenetic Affinities and Phylogenetic Implications

Justin T. Gladman,[1]* Doug M. Boyer,[2] Elwyn L. Simons,[2] and Erik R. Seiffert[3]

[1]*Department of Anthropology, The Graduate Center, City University of New York, New York, NY*
[2]*Department of Evolutionary Anthropology, Duke University, Durham, NC*
[3]*Department of Anatomical Sciences, Health Sciences Center T-8, Stony Brook University, Stony Brook, NY*

KEY WORDS Fayum; Parapithecidae; Platyrrhini; primates; three-dimensional geometric morphometrics; digital surface models

ABSTRACT A well-preserved calcaneus referrable to *Proteopithecus sylviae* from the late Eocene Quarry L-41 in the Fayum Depression, Egypt, provides new evidence relevant to this taxon's uncertain phylogenetic position. We assess morphological affinities of the new specimen using three-dimensional geometric morphometric analyses with a comparative sample of primate calcanei representing major extinct and extant radiations ($n = 58$ genera, 106 specimens). Our analyses reveal that the calcaneal morphology of *Proteopithecus* is most similar to that of the younger Fayum parapithecid *Apidium*. Principal components analysis places *Apidium* and *Proteopithecus* in an intermediate position between primitive euprimates and crown anthropoids, based primarily on landmark configurations corresponding to moderate distal elongation, a more distal position of the peroneal tubercle, and a relatively "unflexed" calcaneal body. *Proteopithecus* and *Apidium* are similar to cercopithecoids and some omomyiforms in having an ectal facet that is more tightly curved, along with a larger degree of proximal calcaneal elongation, whereas other Fayum anthropoids, platyrrhines and adapiforms have a more open facet with less proximal elongation. The similarity to cercopithecoids is most plausibly interpreted as convergence given the less tightly curved ectal facets of stem catarrhines. The primary similarities between *Proteopithecus* and platyrrhines are mainly in the moderate distal elongation and the more distal position of the peroneal tubercle, both of which are not unique to these groups. *Proteopithecus* and *Apidium* exhibit derived anthropoid features, but also a suite of primitive retentions. The calcaneal morphology of *Proteopithecus* is consistent with our cladistic analysis, which places proteopithecids as a sister group of Parapithecoidea. Am J Phys Anthropol 151:372–397, 2013.

Fossils from the late Eocene and early Oligocene sediments of the Fayum Depression, Egypt, continue to provide increased resolution of the morphological changes that occurred along the stem lineage leading to crown anthropoids (e.g., Patel et al., 2012), and critical evidence for resolution of the time and place of origin of several anthropoid clades. Although primate fossils from China and southeast Asia attributed to the families Eosimiidae and Amphipithecidae have suggested to some that stem Anthropoidea did not originate in Afro-Arabia (Beard et al., 1994; Jaeger et al., 1999; Gebo et al., 2000, 2001, 2008; Marivaux et al., 2005; Beard et al., 2007; Chaimanee et al., 2012; Kay, 2012; Seiffert, 2012), the Fayum anthropoid fauna remains the most tangible link between earlier Eocene "prosimians" and later crown members of Anthropoidea, as a number of Fayum taxa are now known from cranial, dental, and postcranial elements (see Seiffert et al., 2010b; Seiffert, 2012 for reviews).

Proteopithecus sylviae is one of only five Fayum anthropoid species that is known from multiple cranial and postcranial elements. The first described specimen of *P. sylviae* was a fragmentary maxilla with teeth that were thought to resemble those of the oligopithecids, *Catopithecus* and *Oligopithecus* (Simons, 1989). Additional discoveries of *P. sylviae*'s upper and lower postcanine dentition revealed that, unlike oligopithecids, the species retained three premolars (Miller and Simons, 1997). The same year, Simons (1997) described two crania of *P. sylviae* that clearly distinguished it from *Catopithecus*, leading him to erect the new Family Proteopithecidae. He also noted dental differences between *P. sylviae* and parapithecids, strengthening the position of *P. sylviae* as the most generalized anthropoid amongst the Fayum taxa known at that time.

Discovery of a partial hindlimb skeleton of *P. sylviae* with associated dental remains added to the growing hypodigm of this taxon (Simons and Seiffert, 1999), with each new element preserving what appears to be a generalized postcranial pattern. The postcranial material

Additional Supporting Information may be found in the online version of this article.

Grant sponsor: National Science Foundation; Grant numbers: BCS-1125507, BCS-1231288, BCS-0819186, BCS-0416164, and DGE-0966166; Grant sponsor: The Leakey Foundation, and contributions from Ann and Gordon Getty.

*Correspondence to: Justin Gladman, Program in Anthropology, The Graduate Center, CUNY 365 5th Avenue, New York, NY 10016-4309. E-mail: JGladman@GC.CUNY.edu

Received 24 October 2012; accepted 24 February 2013

DOI: 10.1002/ajpa.22266
Published online in Wiley Online Library (wileyonlinelibrary.com).

described by Simons and Seiffert (1999), including a femur and two tibiae, exhibited no characters contraindicating stem platyrrhine status, leading the authors to conservatively identify it as the Fayum anthropoid with the best potential to be a stem platyrrhine. Numerous postcranial bones of *Proteopithecus* are now known, including a proximal femur and partial innominate (Gebo et al., 1994), two complete humeri (Seiffert et al., 2000), and an astragalus (Seiffert and Simons, 2001), making it one of the best-known Fayum anthropoids.

Although the number of fossil elements for this taxon has grown, its phylogenetic position within Anthropoidea continues to be debated. A number of recent phylogenetic analyses have supported a stem anthropoid position for *P. sylviae* (Ross et al., 1998; Kay et al., 2004; Seiffert et al., 2004, 2009; Marivaux et al., 2005; Marivaux, 2006; Bajpai et al., 2008; Boyer et al., 2010; Chaimanee et al., 2012), either as a close sister taxon of crown Anthropoidea (Seiffert et al., 2004, 2009), as a basal parapithecoid (Kay et al., 2004; Marivaux et al., 2005; Marivaux, 2006; Bajpai et al., 2008; Chaimanee et al., 2012; Patel et al., 2012), or in either position given slight differences in analytical approaches (Boyer et al., 2010; Seiffert et al., 2010a). Others have suggested a more direct link to platyrrhines, either as a member of the platyrrhine crown group (Takai et al., 2000) or as a member of a parapithecoid sister group of Platyrrhini (Marivaux et al., 2005; Marivaux, 2006). The ambiguity surrounding *P. sylviae*'s phylogenetic position is surely due to the morphological mosaic of primitive and derived characters that are found across the early anthropoid radiation documented in the Fayum, and the realization that several assumed synapomorphies of platyrrhines and catarrhines actually evolved convergently in the two lineages (Seiffert et al., 2004b; Seiffert, 2012), thereby implying a more primitive crown anthropoid ancestor than had previously been envisioned.

Given the ubiquity of mosaicism in fossil taxa, each new bone discovered provides the potential for further clarification of phylogenetic relationships. Here, we describe a complete calcaneus that was found in 2006 at Quarry L-41, a locality that we consider to be terminal Eocene in age (Seiffert, 2006). We attribute this specimen to *P. sylviae*, based primarily on its absolute size and relative abundance at Quarry L-41.

We compare the calcaneus of *P. sylviae* to a broad sample of extant and extinct primates using a three-dimensional geometric morphometric (3DGM) approach. 3DGM has shown great promise for assisting in functional and phylogenetic interpretations of shape variation in isolated postcranial elements (Harmon, 2007, 2009; Drapeau, 2008; Harcourt-Smith et al., 2008; Young, 2008; Holliday et al., 2010; Halenar, 2011; Cooke and Tallman, 2012; Tallman, 2012), and the results reported here will be the first to apply 3DGM methods to the primate calcaneus. We also delimit several calcaneal characters and character states, and employ these features in a large-scale phylogenetic analysis of the early Cenozoic primate radiation in order to rigorously test competing hypotheses of *P. sylviae*'s placement in anthropoid phylogeny and to track calcaneal character transformations among basal anthropoids.

Locality background

Quarry L-41 is situated approximately 48m above the base of a 340m thick section of the Jebel Qatrani Formation exposed north of Birket Qarun in the Fayum Depression, Egypt (Bown and Kraus, 1988). Here, we follow Seiffert (2006), who argued that L-41 is terminal Eocene in age. Given this interpretation, all stratigraphically higher sites in the Jebel Qatrani Formation are early Oligocene (Rupelian) in age.

Institutional abbreviations

AMNH, American Museum of Natural History, New York, NY; CGM, Egyptian Geological Museum, Cairo, Egypt; DPC, Duke Lemur Center Division of Fossil Primates, Durham, NC; GU, H.N.B Garhwal University, Srinagar, Uttarakhand, India; IGM, Museo Geológico del Instituto Nacional de Investigaciones Geológico-Mineras, Bogotá, Colombia; IRSNB, Institut Royal des Sciences Naturelles del Belgique, Brussels, Belgium; KU, Kyoto University, Kyoto, Japan; MCZ, Museum of Comparative Zoology, Harvard University, Cambridge, MA; MNHN, Muséum National d'Histoire Naturelle, Paris, France; NMB, Naturhistorisches Museum Basel, Basel, Switzerland; NMNH, Smithsonian Institution National Museum of Natural History, Washington, DC; NYCEP, New York Consortium in Evolutionary Primatology, New York, NY; SBU, Stony Brook University, Stony Brook, NY; SDNHM, San Diego Natural History Museum, San Diego, California; UCM, University of Colorado Museum of Natural History, Boulder, CO; UCMP, University of California Museum of Paleontology, Berkeley, California; UK, University of Kentucky, Lexington, KY; UM, University of Michigan, Ann Arbor, Michigan; USGS, U.S. Geological Survey, Denver, Colorado.

MATERIALS AND METHODS

Sample

This study includes the new calcaneus attributed to *P. sylviae*, DPC 24776, in a 3DGM analysis with a diverse comparative sample of extant and extinct primates. Taxonomically, this sample is comprised of calcanei from all major extant and extinct primate radiations (Table 1). The sample was collected to maximize genus-level diversity with an emphasis on platyrrhines, which are often considered to retain postcranial features that are more similar to those of extinct basal anthropoids than those of the more specialized extant hominoids and cercopithecoids (Conroy, 1974; Fleagle et al., 1975; Fleagle and Simons, 1982; Fleagle, 1983; Gebo, 1989; Dagosto, 1990; Ford, 1994; Gebo et al., 1994, 2000, 2001; Rose, 1994, 1997).

Methods

Specimen digitization. All analyses are based on 3D surface models of calcanei created by X-ray microcomputed tomographic (microCT) scans at two different institutions (AMNH and SBU). Image stacks from microCT scans of calcanei were transformed into 3D models (specifically Avizo ".surf" files and Stanford ".ply" files) using Avizo software packages. Additional postprocessing was sometimes applied to ".ply" formatted files in Geomagic Studio 12.0 to reduce spike artifacts and fill minor holes (also see Boyer et al., 2010).

Specimen imaging and measurement. DPC 24776 was photographed in stereo using a Leica DVM5000 digital microscope (Fig. 1) and comparative images were

TABLE 1. Taxa and specimens included in the 3DGM analysis

Extant specimen list	*N*	Fossil specimen list
Platyrrhines		Adapiforms
Leontopithecus	2	*Marcgodinotius* (GU 709)
Callimico	2	*Cantius* (AMNH 16852)
Saguinus	4	*Cantius* (USGS 6774)
Callithrix	2	*Cantius* (USGS 6783)
Cebuella	2	*Cantius* (USGS 21829)
Saimiri	5	*Notharctus* (AMNH 55061)
Cebus	2	*Notharctus* (AMNH 11474)
Aotus	3	*Smilodectes* (AMNH 131763)
Callicebus	3	*Smilodectes* (AMNH 131774)
Pithecia	2	
Chiropotes	3	Omomyiforms
Cacajao	2	*Teilhardina* (IRSNB 16786-03)
Alouatta	4	*Washakius* (AMNH 88824)
Ateles	3	*Omomys* (UM 98604)
Brachyteles	1	*Ourayia* (SDNHM 60933)
		Omomyiform (AMNH 29164)
Cercopithecoids		
Macaca	2	Fayum Anthropoids
Cercopithecus	2	Parapithecid (DPC 2381)
Chlorocebus	2	Parapithecid (DPC 8810)
Erythrocebus	1	Parapithecid (DPC 15679)
Mandrillus	1	Parapithecid (DPC 20576)
Lophocebus	1	*Proteopithecus* (DPC 24776)
Theropithecus	1	
Papio	1	Platyrrhines
Colobus	1	*Neosaimiri* (IGM-KU 89201*)
Piliocolobus	2	*Neosaimiri* (IGM-KU 89202*)
Pygathrix	1	*Cebupithecia* (UCMP 38762*)
Nasalis	1	
Trachypithecus	1	Cercopithecoids
		Mesopithecus (MNHN-PIK 266*)
Hominoids		
Hylobates	1	Hominoids
Symphalangus	1	*Oreopithecus* (NMB 37*)
Pongo	1	
Gorilla	1	
Pan	2	
Strepsirrhines		
Daubentonia	1	
Cheirogaleus	1	
Lepilemur	3	
Propithecus	2	
Avahi	1	
Indri	2	
Varecia	1	
Hapalemur	3	
Eulemur	2	
Lemur	3	

Asterisk indicates that only a cast of the actual specimen was available. *N*, number of individuals.

created using 3D models generated from the microCT scans described above.

Several traditional linear and areal measurements were used in this study. To aid in determining taxonomic attribution of the specimen, DMB and ERS took maximum buccolingual and mesiodistal length measurements on mandibular first and second molars of all primates from L-41 (see Supporting Information Table S1 for raw data). DMB and ERS measured 14 of the same specimens and found comparable precision and no systematic offset.

As another component of our approach for determining attribution, JTG measured articular facet areas on the cuboid and ectal facets of the calcaneus, while DMB measured the ectal facet area of the astragalus associated with each calcaneus measured by JTG (see Taxonomic Attribution) (Fig. 2). These areal measurements were taken in Geomagic Studio 12.0. Raw data on facet surface areas are only provided for Fayum anthropoids at this time. Basic linear measurements were taken on scan images in Avizo 6.3 using the 2D measurement tool with "orthographic projection mode" selected for the viewing window (Fig. 3; Table 2).

Taxonomic attribution. Initial observations of DPC 24776 suggested that the bone was likely that of a *Proteopithecus sylviae* individual based on (1) a qualitatively assessed close match between the new calcaneus and the astragalus attributed to *P. sylviae* by Seiffert and Simons (2001) and (2) the fact that *P. sylviae* is one of the most abundant species at L-41. *Catopithecus browni* is comparably abundant, but has astragali that are larger than the single known astragalus of *P. sylviae*, and are therefore too large to articulate with the new calcaneus. We evaluated this hypothesis using regression analyses, in which astragalar ectal facet areas were employed as the independent variable and either calcaneal-cuboid or -ectal facet areas were used as the dependent variables (two regressions) on a sample of extant primates (species: $n = 35$, individuals: $n = 73$; see Supporting Information Table S2 for full list of specimens). We then evaluated whether the astragalar ectal facet areas generated predictions for calcaneal-cuboid and -ectal facet areas with confidence intervals encompassing the observed values of the new calcaneus DPC 24776. To test whether a good fit between the calcaneus and the astragalus was sufficient evidence for the conclusion that the bone belonged to *P. sylviae* to the exclusion of any other L-41 primates (i.e., those lacking an astragalus), we measured all available primate mandibular first and second molars with good taxonomic identifications from L-41 (species: $n = 9$, individuals: $n = 57$), and used PAST to run ANOVA on the natural log-transformed summed area of m1 and m2, assessing whether *P. sylviae* was significantly different in molar dimensions from other L-41 primate species.

3D geometric morphometric analysis. All 3D surface reconstructions were imported into Landmark Editor (Wiley et al., 2005), where the surface morphology is captured in a series of homologous *x*-, *y*-, *z*-coordinates (Bookstein, 1991). A total of 27 landmarks were used in this study based on osteometric points described in previous morphometric studies of the calcaneus (Ford, 1980, 1988) along with a number of novel landmarks (Fig. 2; Appendix A). The full list of specimens included in this study is given in Supporting Information Table S3. Landmarks were registered with respect to one another using a generalized procrustes analysis (GPA) in *morphologika*^{2} (O'Higgins and Jones, 2006). This method minimizes the sums of squared distances between landmarks by eliminating differences in translation, rotation, and scaling (Gower, 1975; Rohlf and Slice, 1990). The result of the GPA is a projection of the multidimensional shape differences into a tangent shape-space where multivariate statistics, such as principal components analysis (PCA) and phenetic clustering algorithms, can be applied—in this case using PAST statistical software (Hammer et al., 2001; Hammer and Harper, 2006). Wireframes created in *morphologika*^{2} were also used to explore the resulting morphospace and highlight the biologically relevant shape changes between groups.

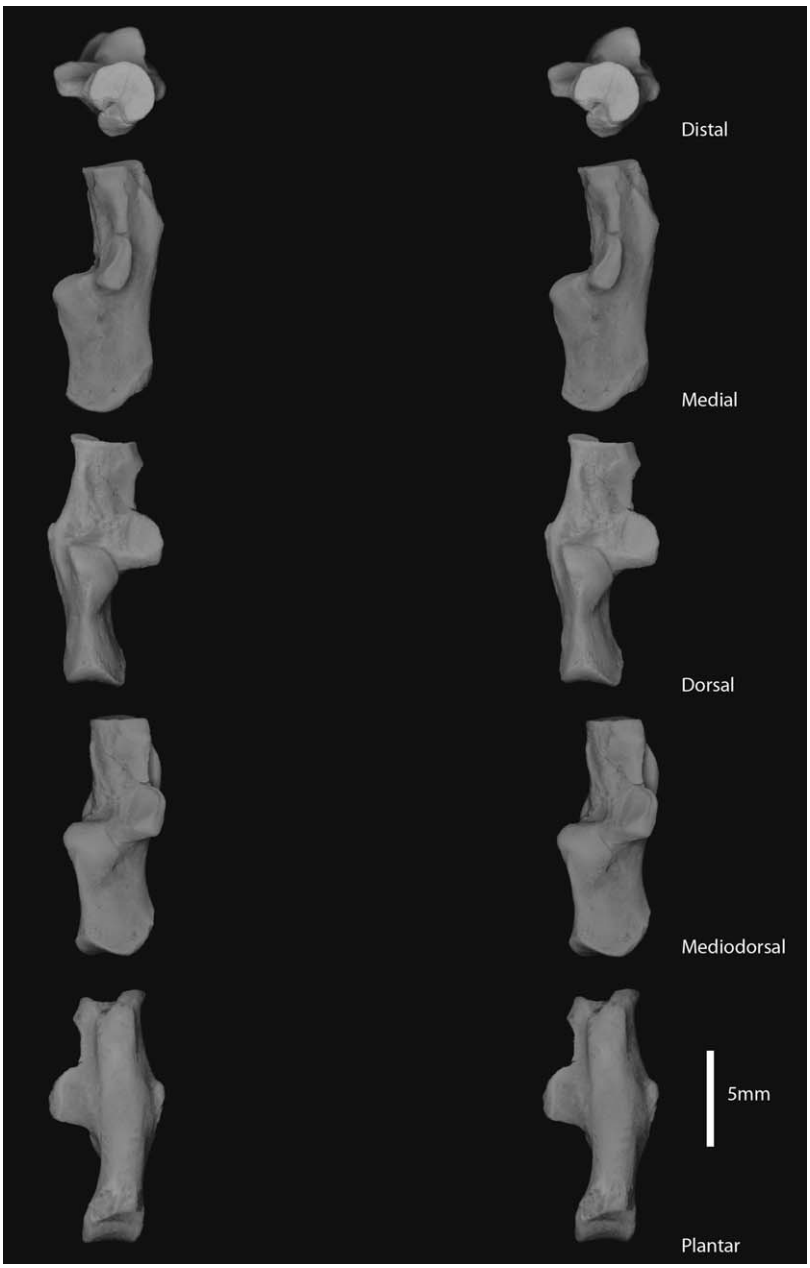

Fig. 1. Stereopair photographs of DPC 24776, *Proteopithecus sylviae* from L-41 quarry.

Along with PCA, which identifies shape variables that account for the maximum variation across the whole sample, our analysis also included a variety of clustering algorithms: Unweighted Pair Group Average (UPGMA), Ward's Method (Ward's), and Neighbor-Joining (NJ) trees to interpret overall phenetic similarities of the sample (e.g., Lockwood et al., 2004; Gilbert, 2011). PCA was performed on all individuals in the sample, to capture the full variability, while clustering algorithms used genus averages of modern taxa in order to avoid any bias in the clustering of large groups of extant specimens compared to smaller groups of fossils. Fossil genera were not averaged together in the clustering analyses in order to increase the sample size of these groups, and because allocations of fossil postcrania to a specific taxon are sometimes provisional.

Cladistic analysis

New calcaneal characters. We explored patterns of shape variation revealed by PCA plots derived from 3DGM analyses to identify and define several new morphological characters on the calcaneus, and to refine calcaneal characters that had been used in previous analyses. We expanded the morphological character matrix used by Patel et al. (2012), which included a total of 373 characters (10 calcaneal), to a total of 391 characters, of which 30 describe variation in calcaneal morphology across the entire Eocene-to-Recent radiation of crown primates. Appendix B provides definitions of these new characters and a list of changes to coding schemes of calcaneal characters that appeared in previous publications. We also expanded taxon sampling over that

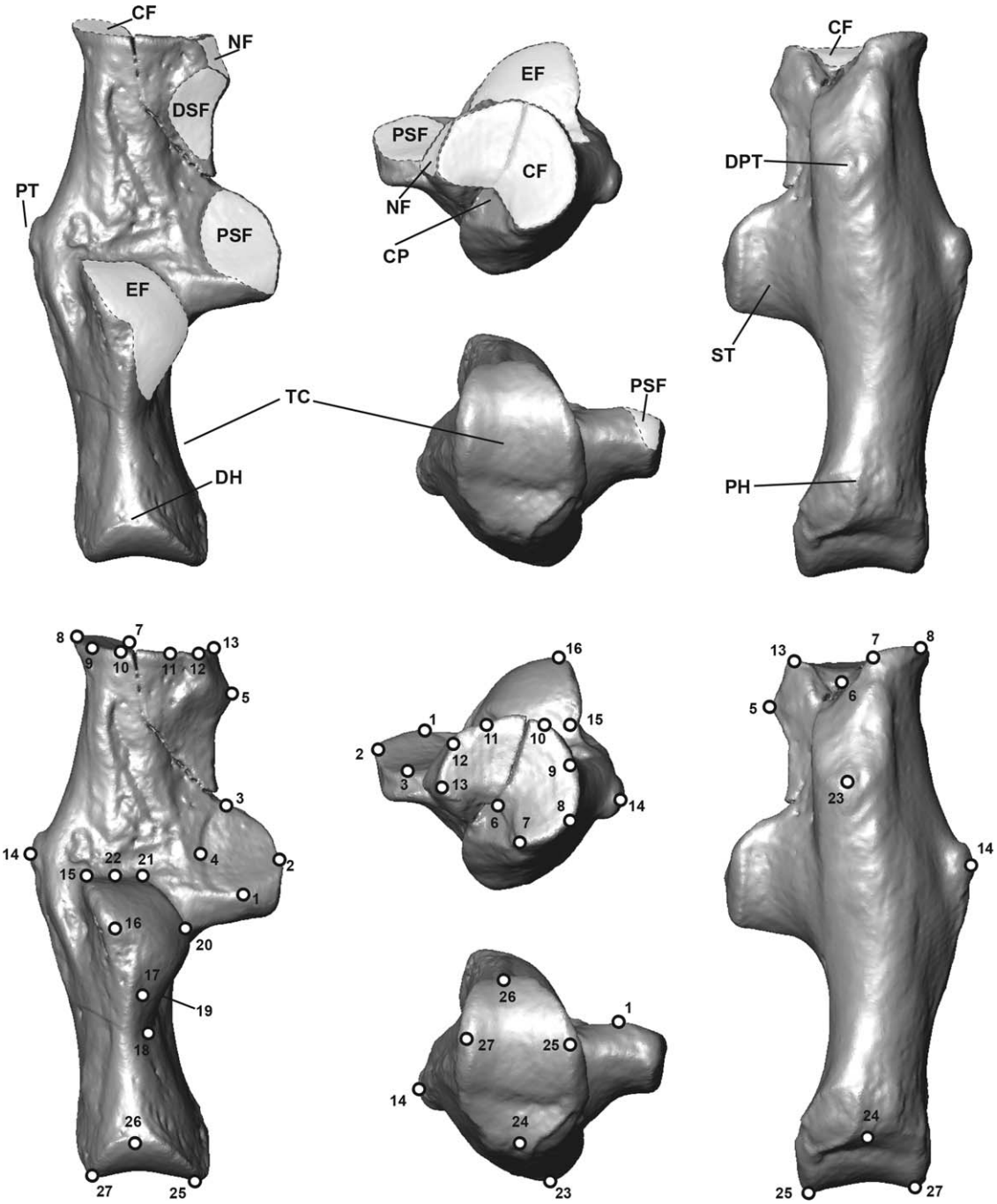

Fig. 2. Anatomical features and 3D landmarks. See Appendix 1 for landmark descriptions. Abbreviations: CF, cuboid facet; CP, cuboid pit; DH, dorsal heel process; DPT, distal plantar tubercle; DSF, distal sustentacular facet; EF, ectal facet; NF, navicular facet; PH, plantar heel process; PSF, proximal sustentacular facet; PT, peroneal tubercle; ST, sustentaculum tali; TC, tuber calcaneus.

used by Patel et al. (2012) by adding an extant hominoid (*Pan troglodytes*), an extant cercopithecoid (*Allenopithecus nigroviridis*), an additional extant platyrrhine (*Alouatta seniculus*), and an additional early Miocene fossil platyrrhine (*Soriacebus*) (note that *Allenopithecus* and *Soriacebus* are not included in 3DGM analyses).

Parsimony analysis. The morphological character matrix used here builds on that which was used in previously published phylogenetic analyses, such as those of Seiffert et al. (2005a,b, 2009, 2010a), Rose et al. (2009), Boyer et al. (2010), Steiper and Seiffert (2012), and Patel et al. (2012). As in those studies, some of the characters in the matrix were treated as ordered, and when polymorphisms were observed between adjacent states in an ordered morphocline, they were scored as an intermediate state rather than using standard polymorphic scoring. To maintain consistent weighting across ordered characters, those characters that included intermediate polymorphic states were downweighted by a half-step (i.e., assigned a weight of 0.5) in the parsimony

analyses. As in previous analyses, transformations in characters relating to premolar number were constrained by step matrices so that premolar teeth could not be reacquired following an earlier loss. Appendix C provides a character matrix with all taxa and their codings for all calcaneal characters.

Two parsimony analyses were performed in *PAUP** 4.0b10 (Phylogenetic Analysis Using Parsimony; Swofford, 2002), using random addition sequence and the tree bisection-reconnection branch-swapping algorithm across 5,000 replicates, for a total of 10,000 replicates. A "molecular scaffold" was enforced for certain extant clades that are strongly supported by molecular sequence data (see for instance the analyses of Perelman et al., 2011), but are not recovered by unconstrained parsimony analysis of morphological data—specifically a Madagascan lemur clade, a cheirogaleid-*Lepilemur* clade, and an *Arctocebus-Perodicticus* clade.

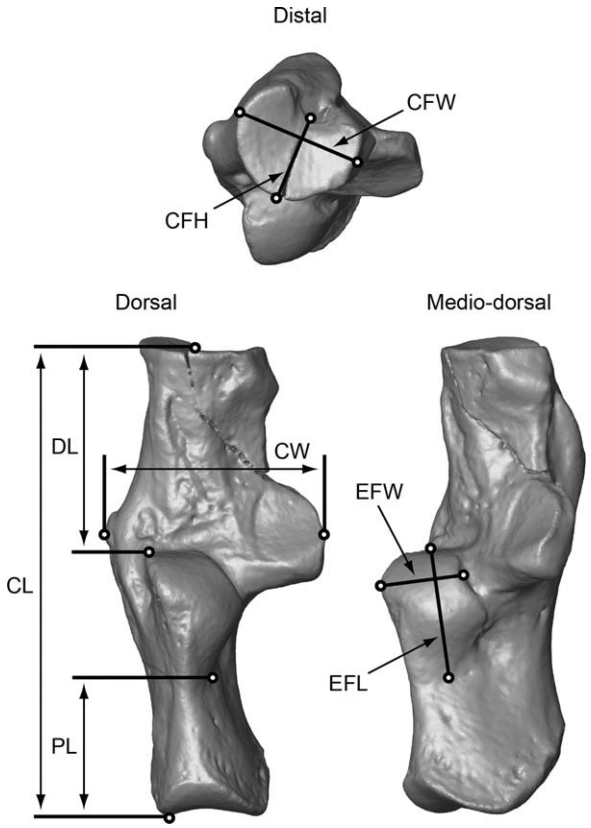

Fig. 3. Linear measurements. See Table 2 for measurements and abbreviation definitions.

RESULTS

Description

The calcaneus of *P. sylviae* (DPC 24776) is moderately wide, with the widest measurement across the sustentaculum and peroneal tubercle being slightly less than half of its total proximodistal length (0.48). The specimen also has moderate distal (0.43) and proximal elongation (0.31), derived from measurements of the length of the calcaneus distal and proximal to the ectal facet, respectively, relative to the total proximodistal length (Table 2). The body of the calcaneus is relatively straight, not bowed in a medio-lateral or dorso-plantar direction. The calcaneus is only very moderately "flexed" at mid-body (i.e., the specimen does not have an ectal facet whose distal margin is deeply depressed into the body of the calcaneus). The distal plantar tubercle is prominent and peaked relatively proximally: in other words, it is set well away from the cuboid facet.

The sustentaculum is somewhat triangular medially and has a defined ridge on its plantar-medial aspect to contain the tendon of *m. flexor fibularis*. Dorsally, the proximal and distal sustentacular facets are separated by a nonarticular region of bone that waists medially back into the body of the calcaneus. The angle between the proximal sustentacular facet and the ectal facet is relatively steep (139°). Distal and plantar to the distal sustentacular facet is a distinct facet, presumably for the lateral margin of the navicular.

The cuboid facet is shallow and fan-shaped with a prominent, medially shifted nonarticular cuboid pit. The long axis of the calcaneocuboid joint is oriented obliquely relative to the mediolateral axis of the calcaneus. The ectal facet is proximo-distally short with a tight radius of curvature. It is not particularly wide, but has a high width/length ratio (0.67) because it is so proximo-distally short. The lateral margin of the ectal facet near the distal terminus does not form a laterally projecting flange,

TABLE 2. Basic measurements (in mm) of Proteopithecus *and other Fayum anthropoids*

Taxon	Specimen #	CL	CW	DL	PL	EFL	EFW	CFH	CFW	EFA	CFA
Proteopithecus	DPC 24776	12.44	6.03	5.41	3.81	3.45	2.31	2.17	3.31	9.06	6.99
Parapithecid	DPC 8810	20.73	11.08	7.82	6.74	6.14	4.03	2.66	5.64	31.58	17.09*
Parapithecid	DPC 15679	21.79	10.52	7.85	7.82	6.01	4.02	3.72	5.61	30.38	21.88
Parapithecid	DPC 2381	21.32	10.75	7.81	7.11	6.29	3.75	2.87	5.85	30.54	19.11
Parapithecid	DPC 20576	15.89	8.14	6.53	4.63	4.69	2.86	2.14*	4.01*	18.69	-
Aegyptopithecus	DPC 10109	–	17.52*	10.8	–	9.59	6.33	4.42	8.6	48.84*	40.99*
Aegyptopithecus	DPC 3051	–	17.65*	11.07	–	9.25	6.42	4.55	7.27*	54.96*	–
"Apidium"	DPC 3833	–	7.75*	–	4.68	5.44	2.72	–	–	20.32	–
Propliopithecus	DPC 1002	–	12.25*	10.22*	–	6.7	3.55*	3.52*	–	25.08*	–
????	DPC 1158	–	–	–	–	5.59*	2.58*	–	–	14.22*	–
"Apidium"	DPC 5416C	–	–	–	–	4.86	2.81*	–	–	–	–
"Apidium"	DPC 24799	23.39	9.98	9.35	8.48	5.7	3.35	2.32*	5.13*	26.87	12.07*
"Apidium"	DPC 24800	–	8.59*	–	–	5.28	2.29	–	–	16.46*	–
????	DPC 14607	–	7.61	6.96	–	4.48	2.82	2.14*	3.19*	14.04*	–

Abbreviations: CL, calcaneus length; CFA, cuboid facet area (see Fig. 2); CFH, cuboid facet height; CFW, cuboid facet width; CW, calcaneal width; DL, distal segment length; EFA, ectal facet area (see Fig. 2); EFL, ectal facet length; EFW, ectal facet width; PL, proximal segment length. See Figure 3 for all linear measurements. Asterisk indicates accuracy-reducing damage to bone.

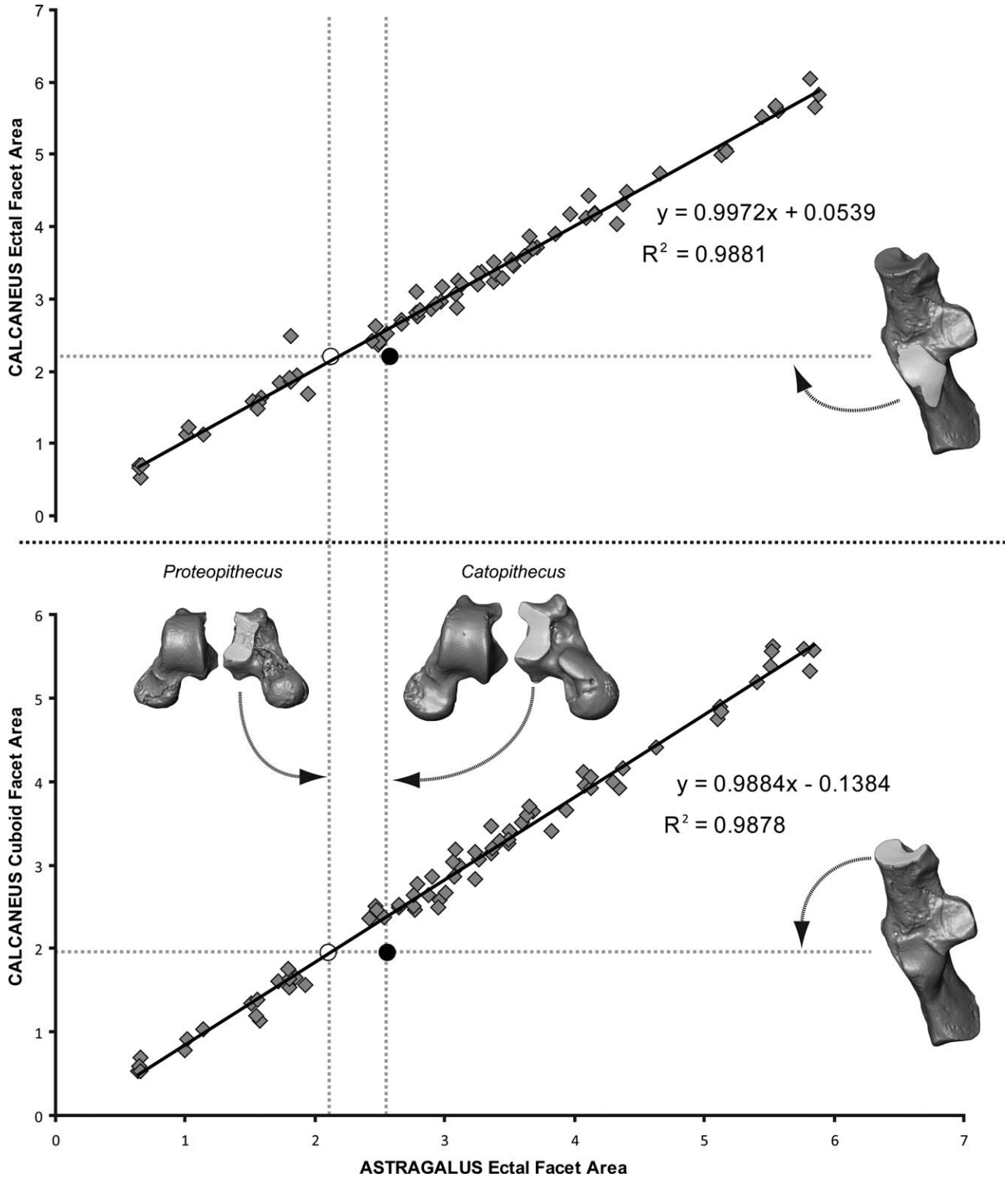

Fig. 4. Regression of astragalus and calcaneus facets. Two different facets of the calcaneus are regressed against ectal facet area of the astragalus for a sample of extant anthropoid and prosimian primates. The tight correlation allows us to assess whether the smaller astragalus of *Proteopithecus* or the larger astragalus of *Catopithecus* is of a more appropriate size to fit with the new calcaneus DPC 24776. Possibility of attribution to the astragalus of *Catopithecus* DPC 22844 is statistically refuted in this way (see Table 3). Note areas were calculated in Geomagic Studio and analyzed as natural logarithms.

or bony extension beyond the supporting bone below (cebines are an example of a group where a laterally projecting flange is prominent). The proximal margin of the ectal facet is poorly differentiated from the supporting bone below, and there is no fibular facet present on the lateral margin of the ectal facet.

TABLE 3. Estimates of calcaneal ectal and cuboid facet sizes derived from known astragalar ectal facets

	Ast-Ect	DPC24776 Cc-prd	LCI	UCI	DPC24776 Cc-obs
Cc Ectal facet					
Catopithecus	2.56	2.61	2.27	2.94	2.20*
Proteopithecus	2.11	2.16	1.82	2.49	2.20
Cc Cuboid facet					
Catopithecus	2.56	2.39	2.06	2.72	1.94*
Proteopithecus	2.11	1.95	1.62	2.28	1.94

Values are natural logarithms of raw measurements. Regression equations used for predictions are shown in Figure 4. Abbreviations: Ast, astragalus; Cc, calcaneus; Ect, ectal; LCI, lower 95% confidence interval; prd, predicted; obs, observed; UCI, upper 95% confidence interval. Asterisk: observed value is below the indicated confidence limit.

The peroneal tubercle is well-developed and has margins that rise gradually (rather than abruptly) from the body of the calcaneus. The maximum lateral projection of the peroneal tubercle is positioned distal to the distal terminus of the ectal facet, and level with the middle to distal half of the sustentaculum. The tuber calcanei is moderately large and rectangular in shape with the insertion of the calcaneal tendon near the plantar surface. The tuber lacks a plantar heel process and the dorsal heel process of the tuber projects up to the level of the ectal facet.

Attribution

At L-41 the most abundant primate fossils are dental remains of *Proteopithecus sylviae* and *Catopithecus browni*, and both of these taxa are represented by numerous postcranial elements (Seiffert et al., 2010b). Other anthropoid taxa represented at this locality are *Abuqatrania basiodontos*, *Arsinoea kallimos*, and *Serapia eocaena*, but these taxa are extremely rare in comparison, and no postcranial remains have yet been attributed to them.

Seiffert and Simons (2001) previously described astragali both of *C. browni* and *P. sylviae*. Our initial impression was that DPC 24776 was of a size that it would fit well with the astragalus of *P. sylviae*, but not *C. browni*. We tested this hypothesis with regression analysis across a sample of 73 primate specimens, and found that astragalar ectal facet area was highly correlated with both calcaneo-ectal and calcaneo-cuboid facets on the calcaneus and had isometric slopes (Fig. 4). Astragalar ectal facet area of *P. sylviae* predicts calcaneal facet areas with confidence intervals that include the values for DPC 24776, while the astragalar ectal facet of *C. browni* yields confidence intervals that do not include the values for DPC 24776 (Table 3).

To assess whether we should expect any of the other Fayum anthropoids to have ankle bones of similar size to those of *P. sylviae*, we measured maximum length and width of all primate m1's and m2's from L-41. To maximize potential for observing differences, we computed the area (length $\times$ width) of each tooth measured for an individual, summed areas of m1 and m2 for each individual, and then took the natural log of the square root of that value. Using *t*-tests, we found that *P. sylviae* ($n = 19$) and *C. browni* ($n = 23$) are significantly different despite overlap (Fig. 5; $F = 1.68$, $t = 7.058$, P[same variance] $= 0.26$, P[same mean] $<< 0.0001$). Furthermore, although sample sizes of specimens for *Abuqatrania* ($n = 2$), *Arsinoea* ($n = 1$), and *Serapia* ($n = 3$) are too small for *t*-tests, all have values in natural log millimeters (*Abuqatrania*: 1.11, *Arsinoea*: 1.24, and *Serapia*: 1.45) that are outside the range of values and 95% confidence intervals of the *P. sylviae* sample (mean: 1.36, CI: 1.34–1.37). Thus, dental evidence does not lead to the prediction that any other Fayum taxon would have had postcranial bones of a similar size to those of *P. sylviae*.

3D geometric morphometric analyses

The first four major principal component (PC) axes account for 65.7% of the total variance in the sample (Figs. 6–8). Examination of the wireframes and distribution of specimens across PC1 (35.9%) reveals a strong association with the overall proportions of the calcaneus, specifically the amount of distal elongation and width/length proportions (Fig. 6A). On one morphological extreme are the distally elongate and narrow-bodied calcanei of omomyiforms and some strepsirrhines, while the distally short and wide hominoid calcanei fall on the opposite end. Distribution of taxa along PC1 compares well with reported figures of distal elongation taken from caliper measurements (Gebo and Simons, 1987; Gebo, 1989; Dagosto, 1990). *P. sylviae* plots with platyrrhines and adapiforms on PC1.

Variation across PC2 (13.6%) is largely explained by the position of the lateral peak of the peroneal tubercle on the body of the calcaneus (Fig. 6B). This variation seems to capture the peroneal position relative to both the ectal facet and the cuboid facet. The Fayum anthropoids are at one extreme on PC2, with a peroneal tubercle that is both distally positioned relative to the ectal facet and also relatively close to the cuboid facet (because the distal segment is only moderately elongated). Some omomyiforms, such as *Teilhardina*, as well as adapiforms, such as *Cantius*, have an even more distally positioned peroneal tubercle relative to ectal facet, but are in a slightly less extreme position on PC2, presumably because of their greater distal elongation.

PC's 3 (9.5%) (Figs. 6, 7A, and 8), and 4 (6.7%) (Fig. 7) represent smaller proportions of the overall sample variation and are also less clearly influenced by a single morphological feature. Both of these PCs capture changes in morphology in the proximal portion of the calcaneus including the amount of proximal calcaneal elongation, the shape and orientation of the ectal facet, and the dorsal projection of the heel (Fig. 6A). In addition, the orientation of the long axis of the cuboid facet also appears to be captured, in part, by PC3. The *P. sylviae* calcaneus groups with hominoids, cercopithecoids, adapiforms and omomyiforms on PC3, which all tend to share similarities of the proximal calcaneus, such as higher levels of proximal elongation, proximo-distally shorter ectal facets, and dorsal margins of the calcaneal tuber that do not project dorsally beyond the ectal facet. Only platyrrhines and most strepsirrhines are clearly different from *P. sylviae* on PC3 with longer ectal facets, more dorsally protruding dorsal margins of the calcaneal tuber, and less proximal elongation. The *P. sylviae* calcaneus groups with most other primates in the sample on PC4, which captures aspects of ectal facet position, curvature and orientation relative to the long axis of the calcaneus. Only adapiforms are clearly distinct from *P. sylviae* and the other Fayum parapithecids, with ectal facets that are more dorsally positioned relative to the calcaneal body.

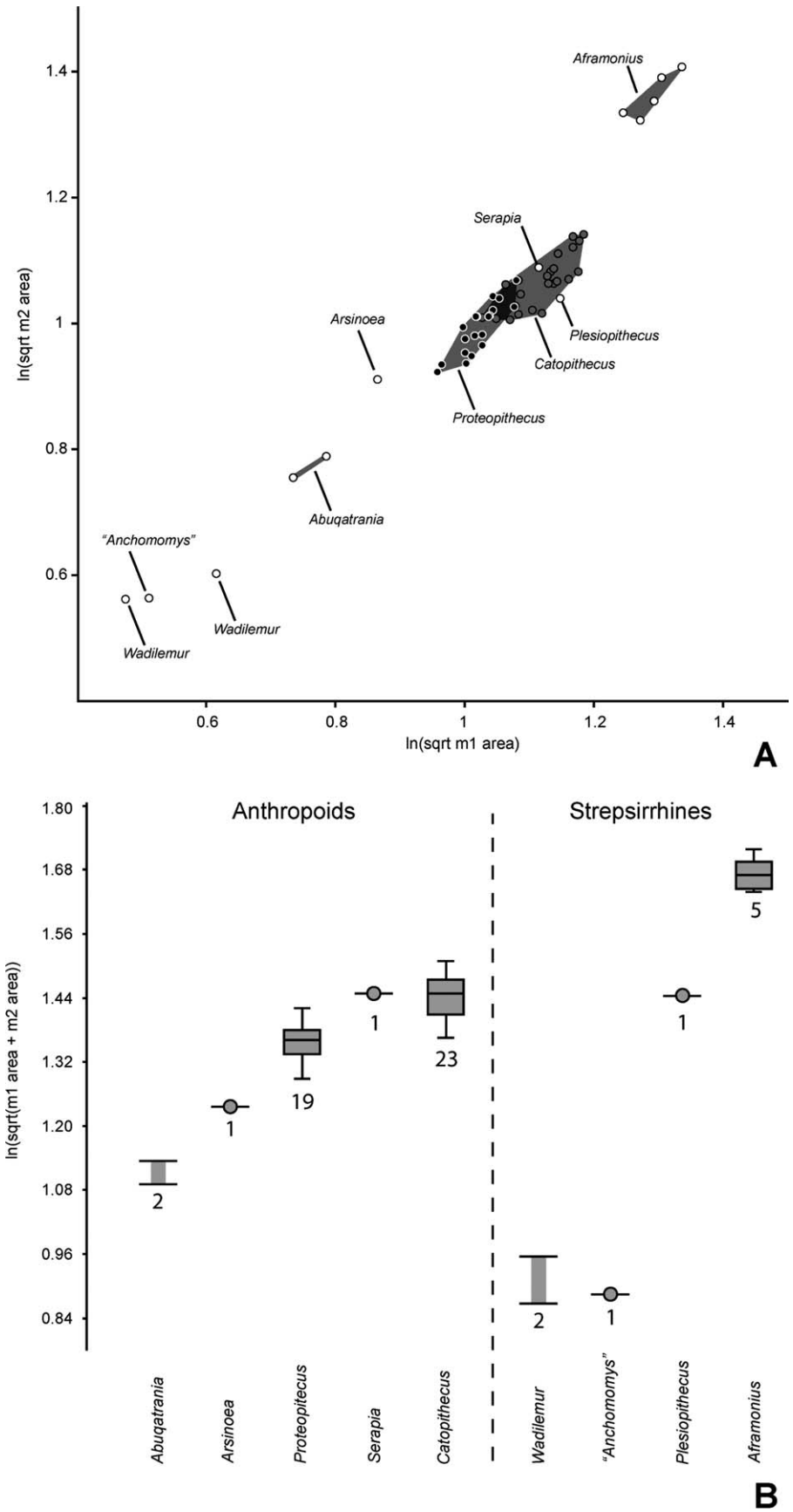

Fig. 5. L-41 primate tooth sizes. Plotting natural log square root of lower molar areas (see methods for details on measurements) shows that *Proteopithecus* overlaps only with *Catopithecus* in dental size among L-41 primates. However, the population means of these two primates are still significantly different (see Results). The only primates that are close in size to *Proteopithecus* are *Arsinoea kallimos* and *Serapia eocaena*, which are both much less abundant at Quarry L-41.

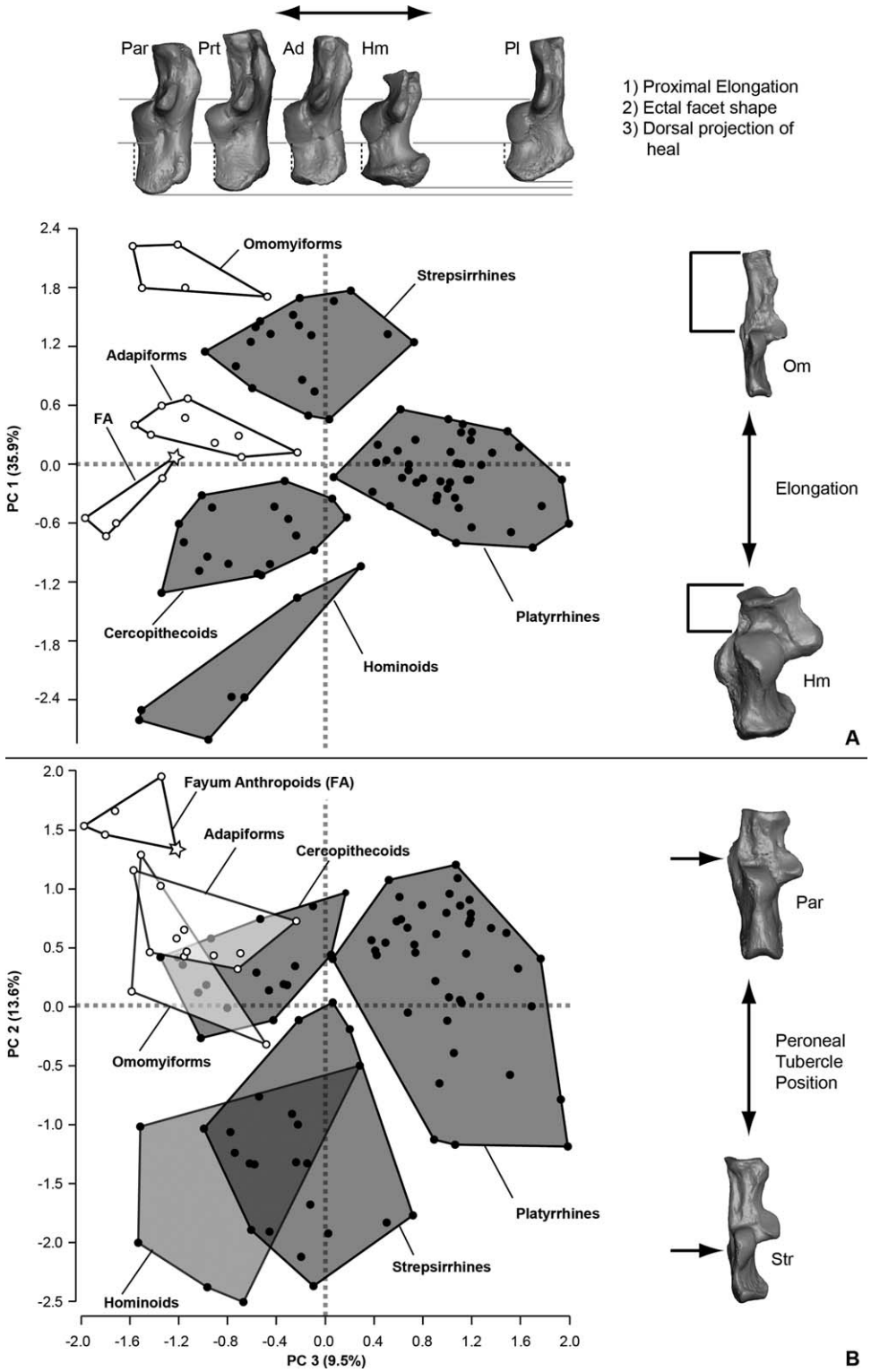

Fig. 6. Principle component plots generated by 3D geometric morphometric analysis of 27 landmarks on the calcaneus (see Fig. 2 and Appendix A). Dark polygons represent extant taxonomic groupings and white polygons represent fossil groups in the analysis. A, Components 1 and 3. Note that PC 1 is correlated with the degree of distal elongation of the calcaneus (see picture). B, Components 2 and 3. Note that PC 2 is correlated strongly with the proximodistal positioning of the peroneal tubercle (see picture). PC 3 is more complex, reflecting more subtle variations in the proximal end, and primarily separates platyrrhines from other primates (see picture). Abbreviations: Ad, adapiform (*Notharctus*); Hm, hominoid (*Pan*); Om, omomyiform (*Washakius*); Par, Parapithecid; Pl, platyrrhine (*Callicebus*); Prt, *Proteopithecus*; Str, Strepsirrhine (*Hapalemur*).

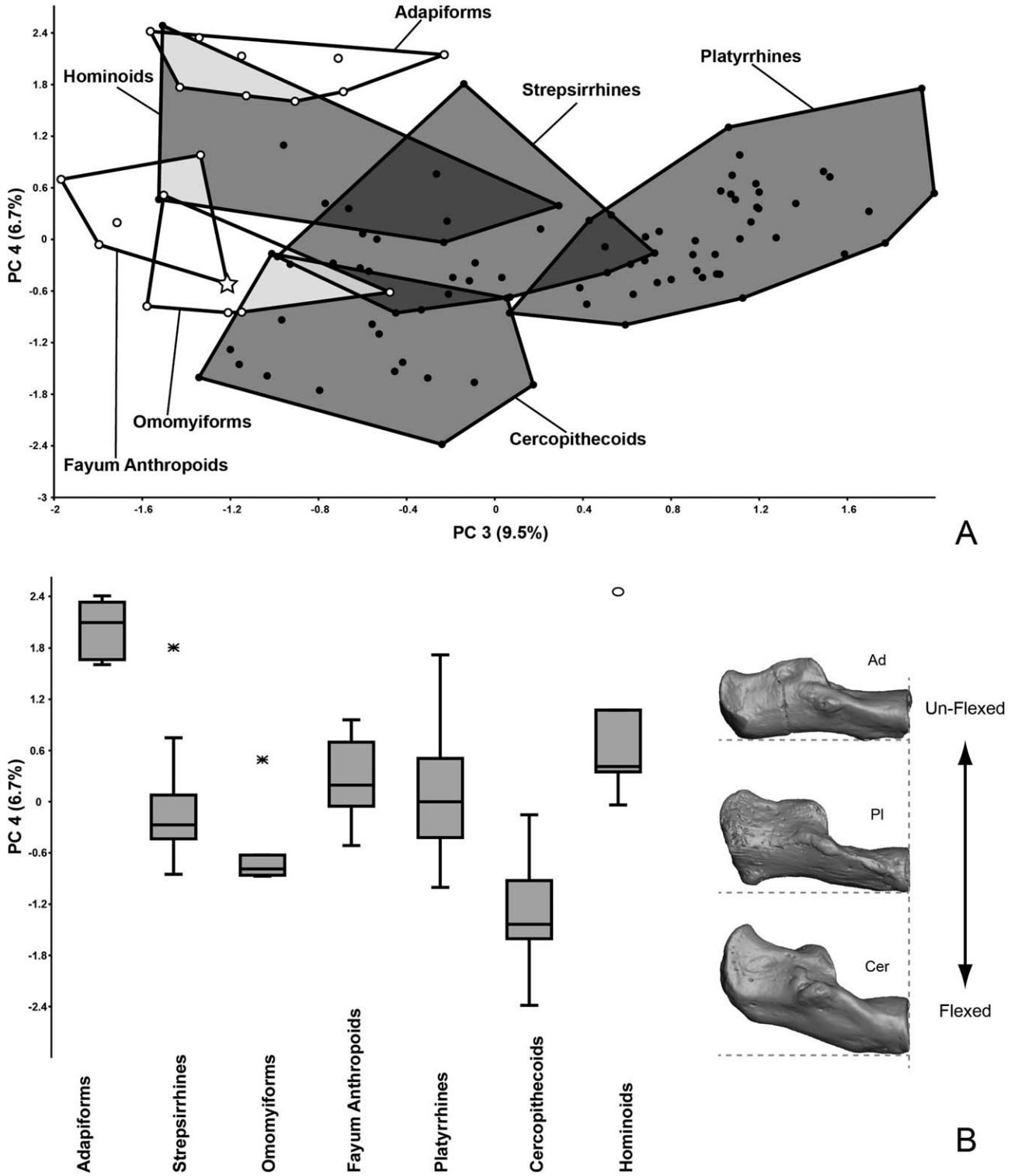

Fig. 7. A, PCA plot of components 3 and 4. B, Box plot of PC 4 scores by clade.

The features described above for PC3 and 4 combine to highlight an overall "flexing" of the calcaneus in which the ectal facet is more flattened plantarly against the body, the dorsal heel process projects more dorsally, and the cuboid facet is oriented more dorsally. This change, along with a medially rotated pivot in the cuboid facet, gives the body of the calcaneus a flexed appearance in lateral view (i.e., dorsally concave/ventrally convex). Individual parts of this overall flexing have been described before, such as the level of the dorsal heel process relative to the ectal facet (Gebo, 1986; Gebo and Simons, 1987), but the suite of changes captured in PC3 and PC4 have never been illustrated in the way presented here.

Combining the separate PC variables in the plots depicted in Figures 6–8 is instructive for assessing the morphological affinities of *P. sylviae* to other primates in

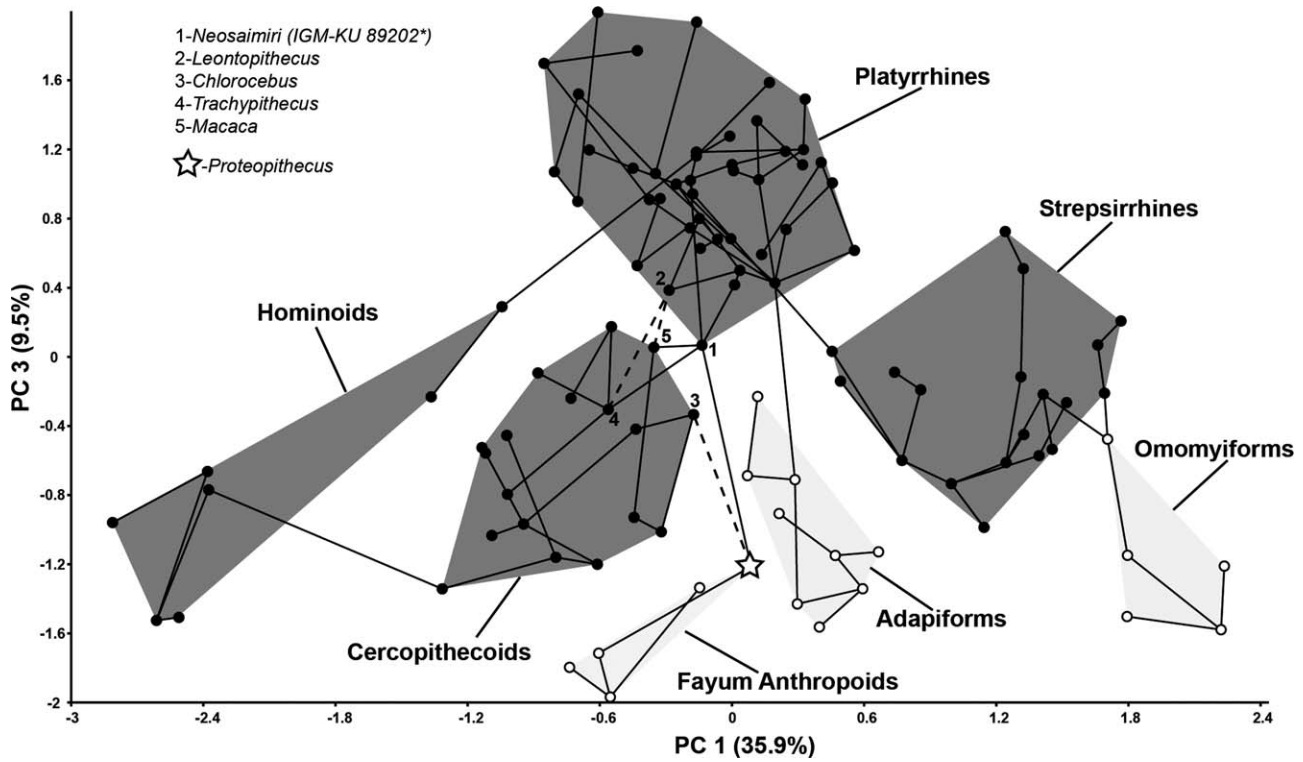

Fig. 8. PCA plot of components 1 and 3 with MST. This figure shows that the morphospace is generally congruent with the actual total morphological distances between specimens as represented by Procrustes distances. Note that hominoids are the only "nonmonophyletic" cluster. Note also that although *Proteopithecus* links to platyrrhines (*Neosaimiri* IGM-KU 89202) among anthropoids, cercopithecoids link to platyrrhines through this same specimen. Interestingly, when *Neosaimiri* is removed from the analysis parapithecids and *Proteopithecus* link to cercopithecoids, leading to the conclusion that *Neosaimiri* might be unusual among platyrrhines.

the sample. In the plot of PC1 versus PC3, which represents a total of 45.4% of the total variation in the sample, there is no overlap among any major clades of primates. In this morphospace, largely representing calcaneal proportions (PC1) and variation in aspects of the ectal facet and tuber shape (PC3), *Proteopithecus* is closest to Fayum parapithecids, followed by adapiforms and some cercopithecoids (Figs. 6A and 8). In the plot of PC2 versus PC3 (Fig. 6B), representing less of the total variation (23.1%), the *P. sylviae* calcaneus is again nearest to Fayum parapithecids, but also close to basal euprimates like *Cantius* and *Teilhardina*. Extant strepsirrhines and haplorhines fall farther away when interpreting only the shape variation captured by PC2 and 3.

Even though the Fayum anthropoids appear distinct from modern anthropoid groups in the PC morphospace (but see PC4), a minimum spanning tree (MST) added to these plots (Fig. 8) links the *P. sylviae* calcaneus to younger Fayum parapithecids and to the Miocene platyrrhine *Neosaimiri* (IGM-KU 89202). The MST is formed by the shortest possible set of lines connecting all points, based on Procrustes distances of the aligned sample. Removing the *Neosaimiri* fossil from the sample only changes three connections of the MST (represented by dashed lines in Fig. 8). In the reduced MST the *P. sylviae* calcaneus links to the cercopithecoid *Chlorocebus*. The other two changes are cercopithecoids (*Trachypithecus* and *Macaca*) that previously connected to *Neosaimiri* and instead link to the extant platyrrhine *Leontopithecus*. In both versions of the PC analysis, the closest links for *P. sylviae*, outside of the other Fayum taxa, are to individuals from crown Anthropoidea.

However, another way to visualize the overall similarity of the calcanei in the sample is to examine generic averages of calcanei in the sample cluster in a phenetic tree, such as the NJ (Fig. 9), UPGMA, or Ward's (Fig. 10). In all of the clustering algorithms the new *P. sylviae* calcaneus groups with parapithecids. This grouping was always essentially "monophyletic" and never included any non-Fayum taxa. The next closest group to the Fayum anthropoids depended on which clustering algorithm was used. In the NJ tree, the Fayum cluster groups within a unified anthropoid cluster, separate from strepsirrhines, omomyiforms and adapiforms. The NJ tree is rooted with a basal adapiform (*Marcgodinotius*), but the same anthropoid cluster is preserved when any other adapiform or omomyiform is chosen. Other fossil anthropoids in the sample group within their expected phylogenetic groups: *Cebupithecia* and *Neosaimiri* with other platyrrhines, *Oreopithecus* with hominoids, and *Mesopithecus* with cercopithecoids. These results support the interpretation that *Proteopithecus* and parapithecids in the sample are phenetically most similar to each other and to extant anthropoids. The UPGMA and Ward's tree maintain a unified Fayum anthropoid grouping, but the next closest cluster in both analyses is the adapiform cluster, probably highlighting the primitive nature of these bones.

Cladistic analyses

Parsimony analysis. Two independent 5,000-replicate parsimony analyses of the 391-character morphological character matrix in *PAUP* 4.0b10 recovered a total of

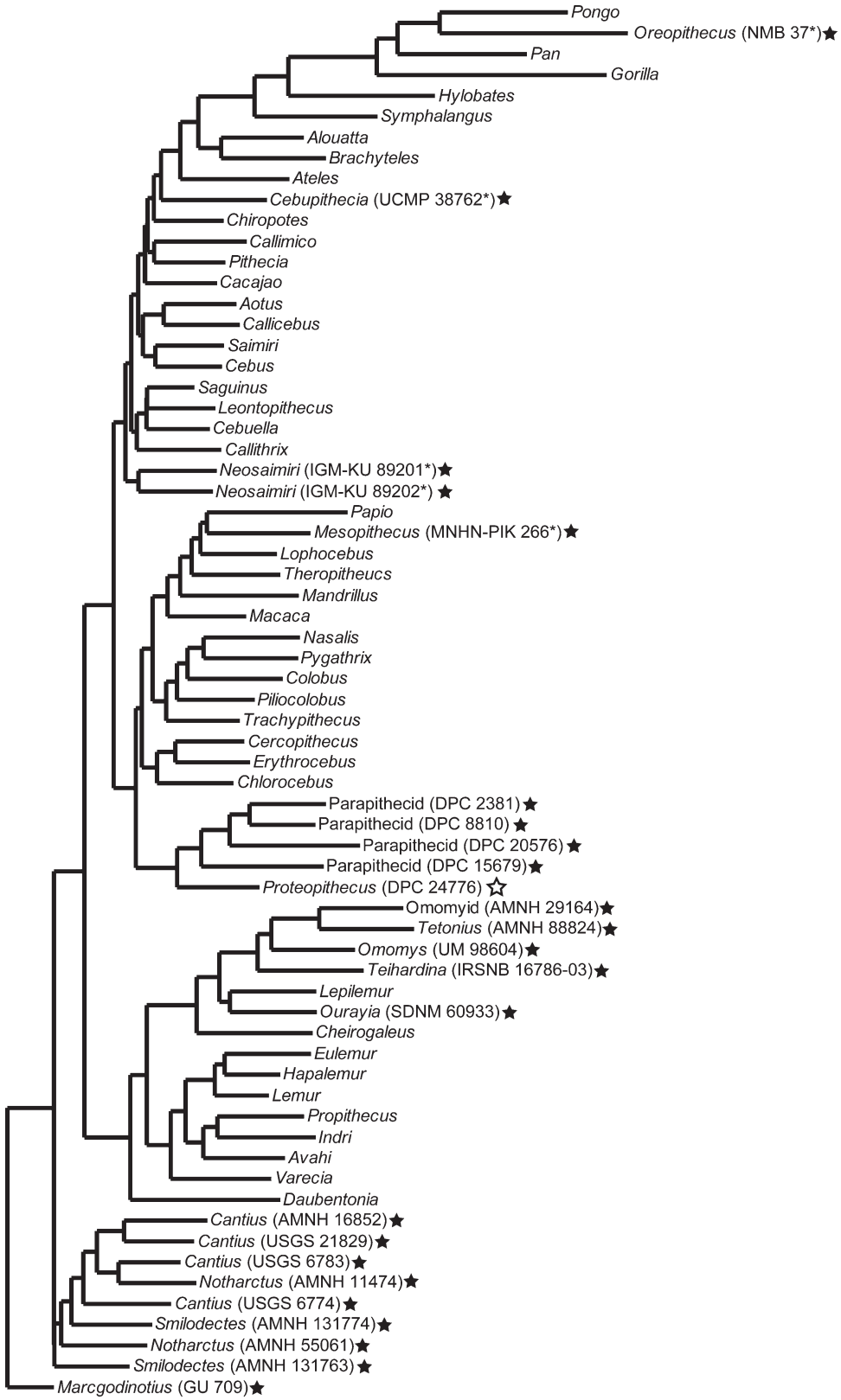

Fig. 9. Neighbor Joining tree. Rooting a comparison of phenetic similarities with a taxon that is likely to be close to the primitive euprimate condition for the calcaneus (*Marcgodinotius*) may help to assess the phylogenetic significance of such similarities. Unlike unrooted clustering analyses (Fig. 10), this approach picks up on derived similarities between parapithecids, *Proteopithecus* and other anthropoids. Conversely, omomyiforms fail to be placed in a phylogenetically reasonable position because the phenetics of their calcanei are dominated by the extreme elongation of the distal segment.

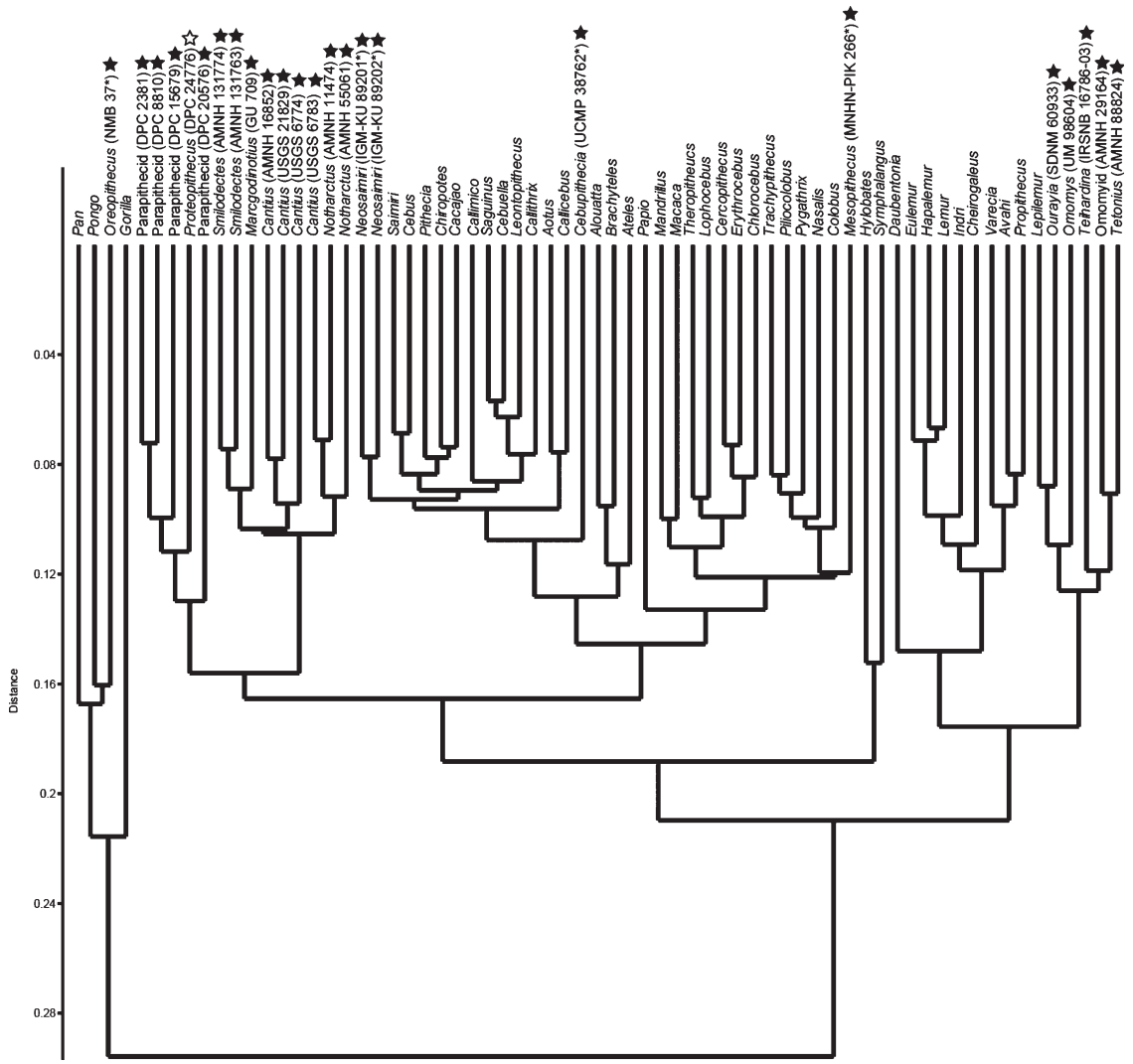

Fig. 10. UPGMA tree (above) and Wards tree (continued on next page). Unrooted clustering reveals phenetic monophyly of parapithecids as well as consistent similarity to adapiforms.

820 equally parsimonious trees of length 4,418 (following re-rooting), 166 of which were unique following collapse of zero-length branches. The Adams consensus of those 166 trees is provided in Supporting Information Figure S1. The consistency index for these trees (excluding uninformative characters) was 0.1582, the retention index was 0.5650, and the rescaled consistency index was 0.0902. Despite the addition of several new calcaneal characters, there are few changes from the results of Patel et al. (2012) for their most comparable analysis (i.e., some characters ordered and scaled [their Supporting Information Fig. S1A]). As in Patel et al.'s analysis, *Proteopithecus* was placed as the sister taxon of contemporaneous and sympatric *Serapia*, followed by the similarly contemporaneous and sympatric *Arsinoea*; this clade in turn formed the sister clade of Parapithecoidea. Within Anthropoidea, the most notable changes from Patel et al.'s result is that amphipithecids are placed as basal stem catarrhines rather than as stem platyrrhines, *Bahinia* is placed in a much more basal position relative to parapithecoids and crown anthropoids, and *Altiatlasius* and *Afrotarsius* are not placed within Eosimiidae but as a more advanced stem anthropoid (*Altiatlasius*) and as a tarsiiform (*Afrotarsius*).

For the purpose of calcaneal character optimizations, following parsimony analysis, all taxa that were not scored for calcaneal characters were deleted from the resulting 166 trees, leaving a total of 46 taxa. A strict consensus was again computed (Fig. 11), leaving a more resolved tree that was not influenced by "wild-card" taxa that could not be placed in a consistent position (e.g., *Xanthorhysis*). The arrangement of taxa in this "trimmed" strict consensus was almost identical to that in the Adams consensus that included all taxa (Supporting Information Fig. S1), with the exception that *Arapahovius* was placed as the sister taxon of an *Absarokius-Tetonius* clade in the Adams consensus. Unambiguous synapomorphies for each node are shown in Figure 11, on which branch lengths are scaled relative to the amount of reconstructed character change. On this trimmed strict consensus of taxa for which calcaneal characters could be scored, the placement of *Proteopithecus* in a clade with Parapithecoidea (represented by *Apidium*) is supported by 22 unambiguous morphological character

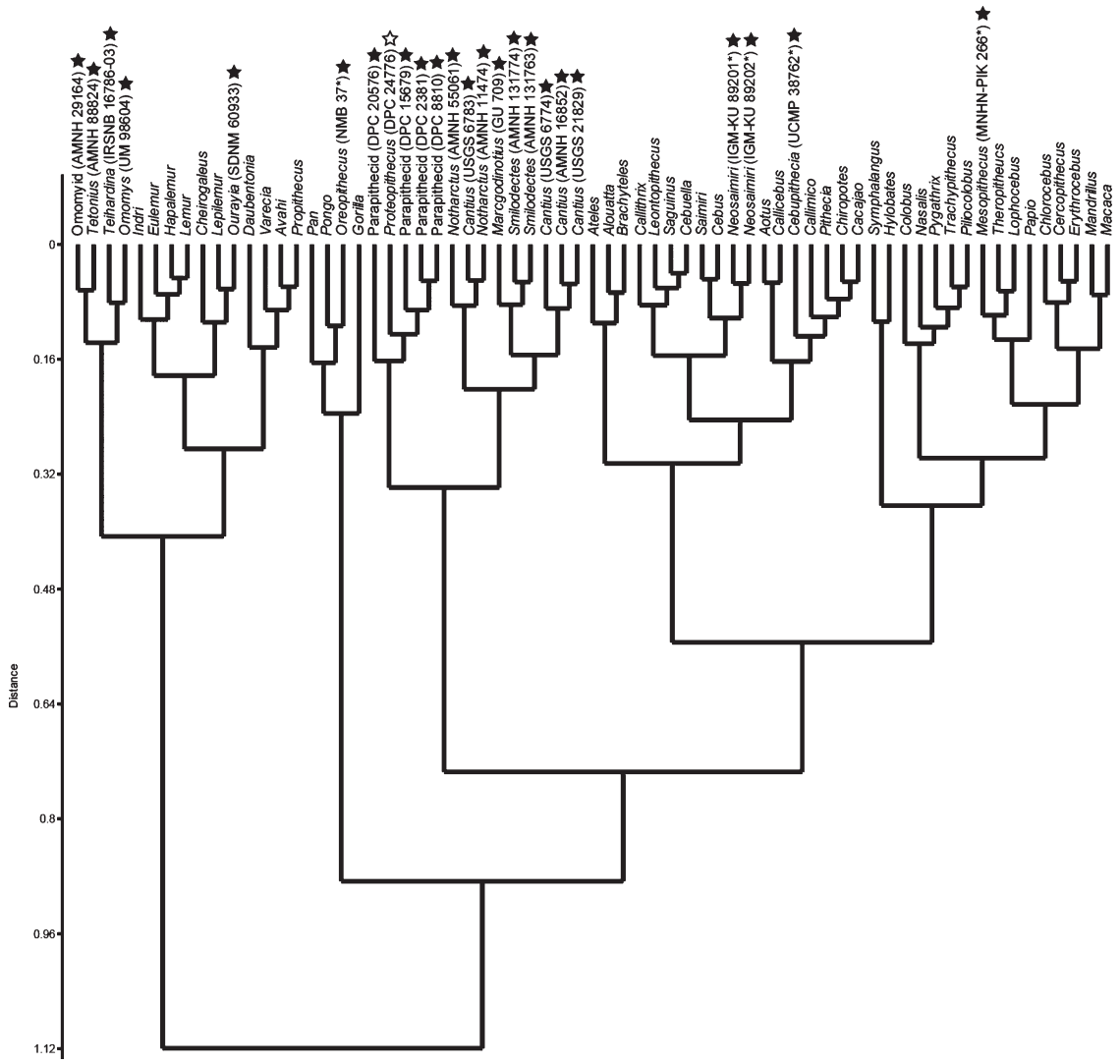

Fig. 10. (Continued)

changes, of which three are calcaneal: "peroneal tubercle level with proximal half of sustentaculum" > "peroneal tubercle level with distal half of sustentaculum" (calcaneal character 11.1 > 11.2), "distal plantar tubercle small and poorly-developed" > "distal plantar tubercle well-developed" (calcaneal character 13.0 > 13.2), and "variable presence of separate proximal and distal sustentacular facets" > "consistent presence of separate proximal and distal sustentacular facets" (calcaneal character 21.1 > 21.2). These characters do, however, show considerable homoplasy across the entire primate tree, with overall consistency indices of 0.133, 0.100, and 0.167, respectively. Crown Anthropoidea is supported by three unambiguous calcaneal synapomorphies to the exclusion of the proteopithecid-parapithecoid clade: "maximum width of peroneal tubercle distal to distal terminus of ectal facet" > "maximum width of peroneal tubercle proximal to the distal terminus of the ectal facet (closer to the distal terminus of the ectal facet than the proximal terminus)" (calcaneal character 12.0 > 12.2); "distal terminus of ectal facet intermediate in position relative to the anterior calcaneal segment" > "distal terminus of ectal facet sunk into body plantarly (i.e., "flexed")" (calcaneal character 27.1 > 27.2); "calcaneal tuber of intermediate size (insertion of calcaneal tendon distinct but not robust)" > "calcaneal tuber relatively robust" (calcaneal character 28.1 > 28.2).

DISCUSSION AND CONCLUSIONS

Attribution

We have demonstrated in a relatively robust statistical framework that 1) DPC 24776 is a better fit for *Proteopithecus sylviae* than *Catopithecus browni* and 2) among Fayum anthropoids smaller than *C. browni*, *P. sylviae* is, on average, dentally larger than any other taxon. However, due to small sample sizes, we were unable to show that differences in dental size statistically reject the possible attribution of the new calcaneus to *Arsinoea kallimos* or *Abuqatrania basiodontos*. Although we think the very large difference in dental size between *P. sylviae* and *A. basidontos* (Fig. 5) provides sufficient quantitative evidence against a possible attribution to the latter taxon, the close similarity in size between *A. kallimos* and *P. sylviae* may be a cause for concern. There is, however, strong contextual

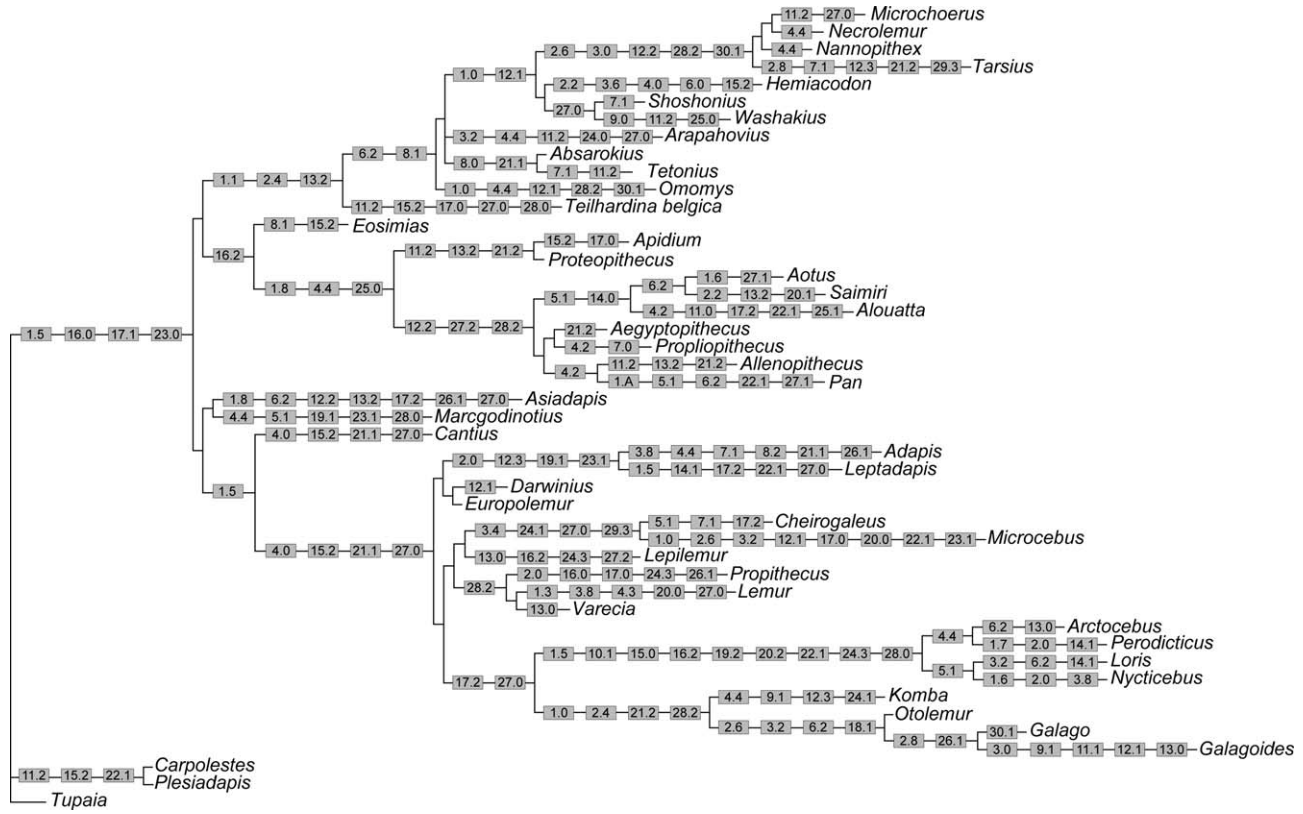

Fig. 11. Relationships of living and extinct primates scored for calcaneal characters. Branch lengths are scaled relative to the number of unambiguous synapomorphies supporting each node. Boxes show the character number followed by the apomorphic character state.

evidence that further reduces the likelihood that DPC 24776 belongs to *Arsinoea*.

There are ~100 craniodental remains of *P. sylviae*, but only two specimens of *A. kallimos* have been discovered since L-41 became an active quarry in 1983 (a description of a new partial maxilla of *Arsinoea* is currently in preparation). Taking the cumulative sample into consideration, finding a *P. sylviae* craniodental element is ~50 times more likely than finding an element of *A. kallimos*. If taphonomic processes involved in deposition of *P. sylviae* and *A. kallimos* remains are similar, sheer abundance suggests that DPC 24776 is ~50 times more likely to be *P. sylviae* than *A. kallimos*. Considering the situation slightly differently, *P. sylviae* is known from 10 postcranial bones, so there are 10 times as many craniodental remains of *P. sylviae* relative to postcranial remains. That means, for a given primate taxon, one can expect on average to find one postcranial element for every 10 craniodental elements discovered. Given that only two *A. kallimos* specimens are known from L-41, it is unlikely that isolated postcranial bones of this species have been discovered yet.

Despite the very small chance that this bone belongs to *A. kallimos* instead of *P. sylviae*, it is important that this attribution, in fact, does not change the phylogenetic implications for the pattern of evolution in calcaneal morphology if this element belongs to *A. kallimos*. This is because *Arsinoea* is placed as the sister group of Proteopithecidae in our analyses, and has been placed either in a similar position, or as a basal parapithecoid with proteopithecids as a parapithecoid sister taxon, in previous analyses (Marivaux et al., 2005; Seiffert et al., 2005b, 2009, 2010a; Bajpai et al., 2008).

Phylogenetic implications of phenetic affinities

The most definitive signal in our 3DGM morphometric analysis is the affinity of the new calcaneus to those attributed to parapithecids from early Oligocene sites in the Fayum (Figs. 6–10). This undeniable affinity could be due to convergence, synapomorphy, or symplesiomorphy; but, given the placement of proteopithecids as the sister group of Parapithecoidea in our analysis, the most parsimonious explanation is a combination of synapomorphies due to relatively recent common ancestry (distal placement of the peroneal tubercle, presence of a distinct distal plantar tubercle, and presence of separate proximal and distal sustentacular facets) and plesiomorphies that are not seen in crown anthropoids. We have no basis for considering convergence as a possible explanation based on available phylogenetic evidence. The consistent tendency of parapithecids and *Proteopithecus* to cluster with adapiform calcanei when no rooting is applied to the clustering algorithm (Fig. 10), or to plot nearest these taxa and/or omomyiforms on PC2–4 of the 3DGM analyses, does indicate that, despite their shared apomorphies, the overall pattern exhibited by parapithecids and proteopithecids might be more reflective of the primitive condition for advanced stem anthropoids than what is seen in the anthropoid crown clade.

The ways in which *Proteopithecus* differs from parapithecids make it slightly more like the sampled adapiforms and omomyiforms in overall morphology and proportions (i.e., a more slender bone with relatively greater distal elongation). One of the distinctive features it shares with parapithecids is also very similar to the condition seen in some omomyiforms (*Omomys*

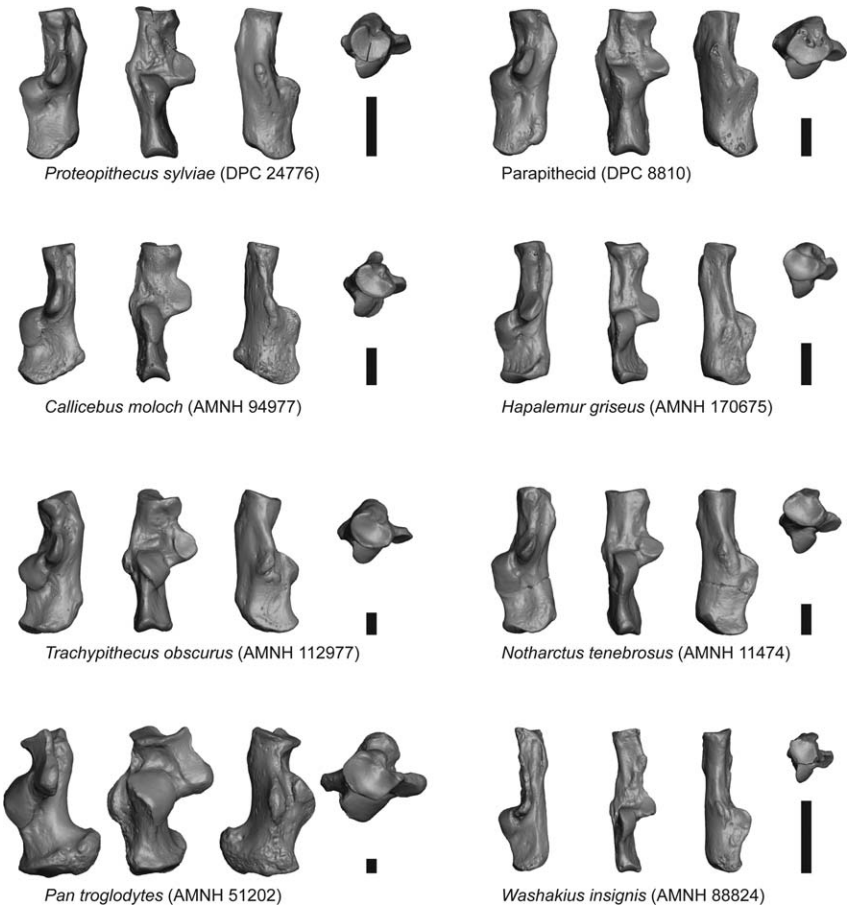

Fig. 12. Comparative images. Representatives of major clades included in this analysis are shown in four views for comparison with each other and *Proteopithecus*. Views are medial, dorsal, lateral, and distal (from left to right). Scale = 5 mm.

specifically)—the ectal facet is proportionally short proximodistally and more tightly curved (i.e., exhibiting a greater arc) compared to those of many primates. Interestingly, eosimiids do not appear to exhibit such tight curvature of the ectal facet, leading one to question the homology of this observed similarity to omomyiforms. Conversely, *Proteopithecus*, *Omomys*, and some eosimiid calcanei exhibit a similar, unusual pattern of ridges and grooves on the dorsal body of the calcaneus (not quantified in any way by our analyses). We find virtually no differences between the calcaneus of *Proteopithecus* and many *Omomys* calcanei from the peroneal tubercle to the heel, (Figs. 13 and 14) with the exception of the more cercopithecoid-like discontinuous proximal and distal sustentacular facets in *Proteopithecus*. Transforming the calcaneus of *Omomys* into the morphology of *Proteopithecus* involves changes mainly to the distal end, including shortening the distal end, changing the cuboid facet orientation from slightly plantar and lateral (in omomyiforms) to more dorsal and medial, and changing the cuboid facet by increasing the depth of the plantar pit and making it nonarticular so that the facet has a "bean-shaped" outline. Despite these morphological similarities between *Proteopithecus* and *Omomys*, our phylogenetic analysis suggests that all known omomyiforms are more closely related to tarsiers than to anthropoids, with more extreme distal elongation being a synapomorphy of an omomyiform-tarsiid clade. This would suggest that the structural transformations described above did not actually happen as part of the evolutionary origin of *Proteopithecus* from an omomyid-like ancestor. The last common ancestor of crown primates is reconstructed as having had only a moderately elongate calcaneus (with calcaneal width between 40 and 50% of length, as in basal stem strepsirrhines [*Cantius*, *Marcgodinotius*] and basal stem anthropoids [*Eosimias*]). A more likely scenario, given these optimizations, is that the common ancestor of *Proteopithecus* and *Eosimias* had a calcaneus essentially similar to that of *Eosimias*.

Gebo and Simons (1987) have also noted that parapithecids exhibit strong similarities to cercopithecoids in their calcaneal morphology. We recovered this signal in our rooted NJ analyses. Ectal facet shape, disjunct proximal and distal sustentacular facets, and cuboid facet orientation all contribute to this signal. Although it is possible that these similarities are primitive retentions in cercopithecoids from a parapithecid-like ancestor, we consider this unlikely due to the fact that parapithecoids are placed outside of crown Anthropoidea in our phylogenetic analyses, and that this morphology is lacking in platyrrhines and the basal stem catarrhine, *Aegyptopithecus* (Gebo and Simons, 1987; Strasser, 1988). The relatively more "open" ectal facet of platyrrhines, *Aegyptopithecus*, many early Miocene catarrhines, and extant hominoids suggests that this was the primitive condition for crown Anthropoidea. The calcaneal morphology of the basal stem catarrhine *Catopithecus* is not known, but its astragalar ectal facet also appears to be more "open" than that of *Proteopithecus* (but this has not

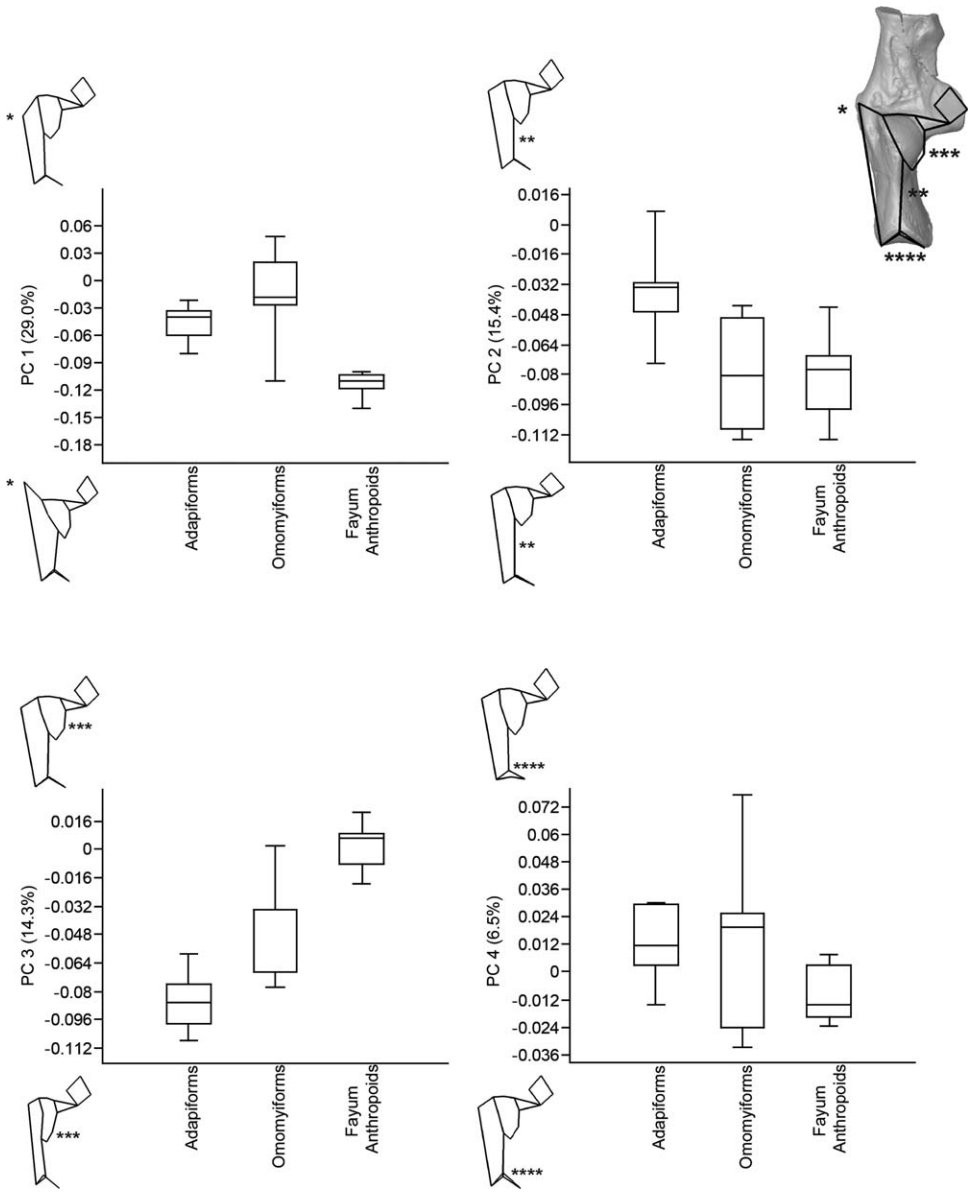

Fig. 13. PCA scores after analysis with nondistal landmarks only. To evaluate affinities without the influence of distal elongation, a PCA was run excluding landmarks #5, #6–13, and #23. Note that Fayum anthropoids (including only *Proteopithecus* and parapithecids) tend to be closer to the mean value of omomyiforms and/or overlap more with omomyiforms than adapiforms. The reverse was true when distal landmarks were included in previous analyses. Asterisks highlight the region that is most variable for each PC axis.

been quantified as it has in the calcaneus). These facts may lead one to question then whether 1) the strong curvature in the ectal facet of parapithecids is homologous to that of omomyiforms, or alternatively, whether 2) the more open facet in the basal crown anthropoid is homologous with that in eosimiids and adapiforms (note that these comprise alternative scenarios only if omomyiforms are treated as a monophyletic clade, or if adapiforms are treated as more closely related to anthropoids than are omomyiforms). The first scenario requires only two instances of evolving tightly curved facets, but also two instances of evolving more open facets (four changes). The latter scenario is actually more parsimonious, only requiring three instances of evolution of tightly curved facets. Even though the phylogenetic conditions for the latter scenario are unlikely, it is useful to entertain the question of why we might see frequent homoplasy in the shape of the ectal facet.

Functional interpretation

Previous interpretations of *Proteopithecus*' locomotor behavior have reconstructed this small-bodied anthropoid as relying on rapid or agile quadrupedal locomotion, likely including some pronograde leaping (Gebo et al., 1994; Simons and Seiffert, 1999; Seiffert et al., 2000; Seiffert and Simons, 2001; Ryan et al., 2012). The calcaneus described here has no morphology that would suggest any alternative mode of locomotion, such as specialized climbing, as it lacks any bowing of the calcaneus, dorsally elevated ectal facet (Gebo, 1988), or presence of a plantar heel process (Sarmiento, 1983). The calcaneus does exhibit a number of features that are consistent with its reconstruction as an arboreal quadruped with leaping capabilities, especially in the tightly curved ectal facet, disjunct proximal and distal

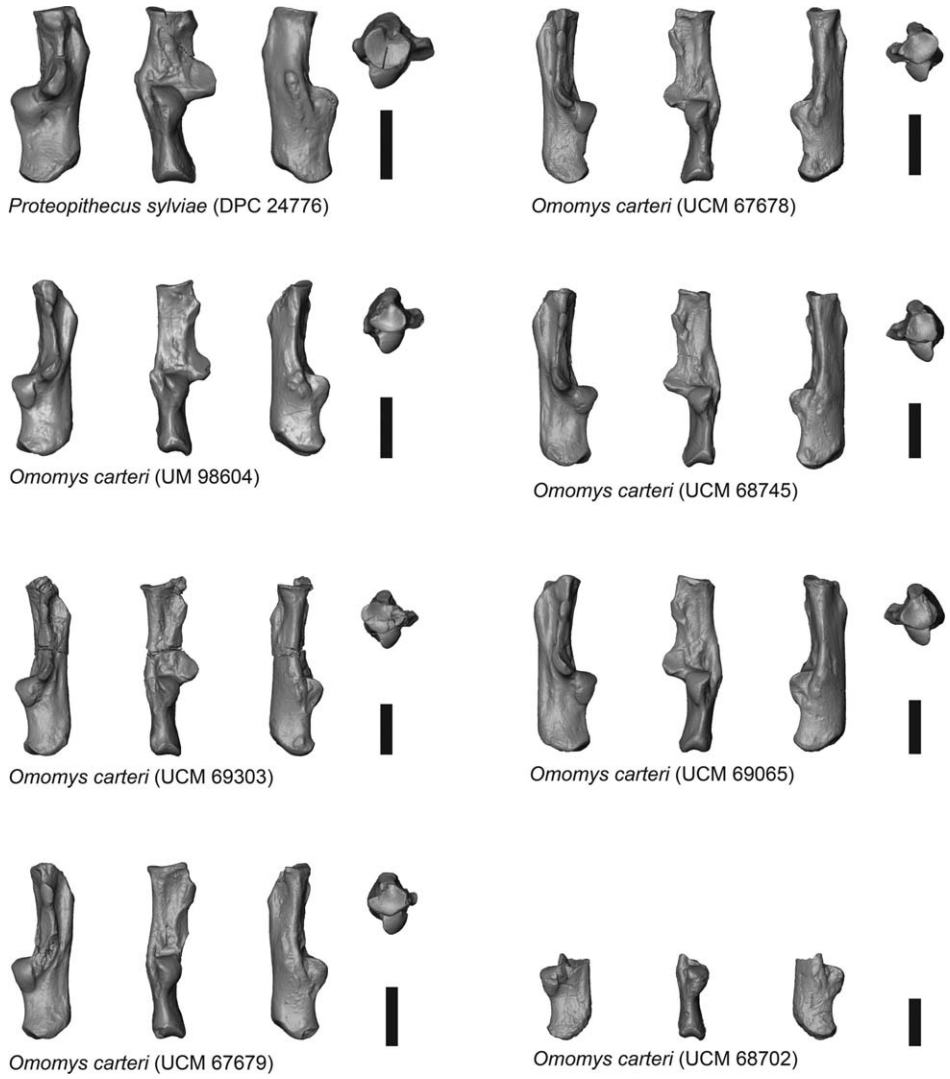

Fig. 14. Comparison of *Proteopithecus* calcaneus to several *Omomys* calcanei to show aspects of similarity.

sustentacular facets, and moderate amount of distal elongation (Langdon, 1986; Gebo, 1988; Strasser, 1988). The first two of these features should reduce astragalocalcaneal joint mobility. The third is consistent with elongating the hind limb generally to help increase takeoff velocities when leaping. However, Moyà-Solà et al. (2011) recently challenged the use of distal elongation ratios as a good metric of leaping in primates, suggesting instead that distal elongation in the primate calcaneus represents a biomechanical tradeoff to maintain adequate leverage action in the foot during locomotion as the fulcrum of the foot shifts from a metatarsi- to a tarsi-fulcrimating position and the load arm is reduced. According to these authors, only the most elongated primate forms, such as tarsiers and galagos, have elongation beyond that explained by the biomechanical tradeoff for hallucial grasping and so can confidently be called leapers.

More suggestive of some leaping capabilities in *Proteopithecus* are the short and tightly curved ectal facet, together with the discontinuous proximal and distal sustentacular facets, which limit flexibility at the astragalocalcaneal joint by restricting the screw-like motion of the astragalus on the calcaneus. In a taxon with a more open ectal facet and continuous sustentacular facets (which are also "helically" arranged, Szalay and Decker, 1974), a close-packed position between the astragalus, calcaneus and navicular can be maintained, while the calcaneus is rotated under the astragalus resulting in a stable inverted foot posture (Langdon, 1986; Strasser, 1988). The features of the calcaneus that reduce its mobility on the astragalus are beneficial for taxa that do not require extensive abduction, adduction and eversion-inversion, such as for quadrupedal terrestrial cercopithecoids that stand to benefit from stereotypically fore-aft (flexion-extension) movements (Strasser, 1988). In the arboreal environment that *Proteopithecus* was living these flexibility restrictions are more analogous to morphology found in omomyiform calcanei, which likely stabilized the ankle during fore-aft propulsion when initiating leaping. The combination of these facets in *Proteopithecus*, as well as *Apidium*, might represent leaping adaptations (conforming to interpretations from other regions of their postcranial skeletons) and/or ancestry from an omomyiform-like leaping ancestor (although this latter explanation is less feasible if the stem placement of *Eosimias* is correct).

SUMMARY AND FUTURE DIRECTIONS

On the basis of relative size and abundance, we have attributed the calcaneus DPC 24776 to the terminal

Eocene anthropoid *Proteopithecus sylviae*. Our 3D geometric morphometric and phylogenetic analyses of the specimen provide additional evidence for the parapithecoid affinities of proteopithecids, as had been suggested previously by some parsimony analyses that incorporated the craniodental, humeral, femoral, tibial, and astragalar morphology of *Proteopithecus*. If proteopithecids and parapithecoids do indeed share a common ancestor to the exclusion of crown anthropoids, the divergence between proteopithecids and parapithecoids must be ancient—at least middle Eocene in age, because the basal parapithecoid *Biretia* occurs at the earliest late Eocene locality BQ-2. In light of the considerable differences in dental morphology between *Proteopithecus* and *Biretia*, recovery of additional basal anthropoid postcrania, from Afro-Arabia and Asia, will be critical for further testing this and other phylogenetic hypotheses related to the origin of Anthropoidea. DPC 24776 does not appear to share calcaneal features uniquely with platyrrhines, but does exhibit some characters that are also seen in adapiforms, omomyiforms and cercopithecoids. The features that *Proteopithecus* shares with adapiforms and omomyiforms probably reflect the overall primitive nature of its calcaneus, while similarities to cercopithecoids arguably reflect the convergent evolution of a subtalar ankle joint that was relatively immobile. This pattern was taken to a greater extreme later in the Oligocene in parapithecids such as *Apidium*.

ACKNOWLEDGMENTS

Paleontological work in the Fayum area took place in collaboration with scientists at the Egyptian Mineral Resources Authority, the Egyptian Geological Museum, and the Egyptian Environmental Affairs Agency. The authors thank the staff of these agencies for supporting and facilitating this research, and members of past Fayum field crews for their assistance with excavation at Quarry L-41. Fieldwork was managed by Prithijit Chatrath. The authors thank C.T. Rubin and S. Judex for access to microCT scanning facilities in the Center for Biotechnology of SBU, and to J. Thostenson and M. Hill for access to microCT scanning facilities in the Microscopy and Imaging Facility of AMNH. The authors would also like to thank Eric Delson, Alfred Rosenberger, and Andrew Deane for access to specimens included in this project. They thank a number of students at Brooklyn College, CUNY for reconstructing digital imagery of bones that were used in this study including J. Butler, A. Garberg, and J. Lovoi. M. Steiper provided access to computing facilities. This is Duke Lemur Center publication #1242 and NYCEP Morphometrics Group publication #72.

APPENDIX: A

APPENDIX A. DESCRIPTION OF 3D LANDMARKS

#	Description
1	The proximal-most point on the proximal sustentacular facet, not including any plantar extension.
2	The medial-most point on the border of the proximal sustentacular facet.
3	The distal-most point on the border of the proximal sustentacular facet.
4	The lateral-most point on the border of the proximal sustentacular facet.
5	The medial-most point on the border between the distal sustentacular facet and the proximal portion of the navicular facet.
6	The most dorsal point of the cuboid facet on the plantar border.
7	The most distal point before the cuboid facet lateral-plantar border slopes proximally toward the calcaneal pit.
8	The lateral-most point on the long axis of the cuboid facet.
9	The point on the medio-dorsal border of the cuboid facet that forms a perpendicular line with landmark 7 relative to the long axis of the cuboid facet (landmarks 8 and 12)
10	The dorsal point that forms a perpendicular line with landmark 6 relative to the long axis of the cuboid facet (landmarks 8 and 12)
11	The point on the latero-dorsal border of the cuboid facet that forms a perpendicular line with landmark 13 relative to the long axis of the cuboid facet (landmarks 8 and 12)
12	The medial-most point on the long axis of the cuboid facet.
13	The most distal point before the cuboid facet medial-plantar border slopes proximally toward the calcaneal pit.
14	The lateral-most point of the peroneal tubercle.
15	The intersection of the lateral border of the ectal facet and the body of the calcaneus at the ectal facet distal terminus.
16	The dorsal-most point of the lateral border of the ectal facet.
17	The point where the lateral border of the ectal facet begins to join with the body at the proximal terminus.
18	The center or most proximal extension of the proximal border of the ectal facet.
19	The point where the medial border of the ectal facet begins to join with the body at the proximal terminus.
20	The point almost directly medial to landmark 16, positioned on the medial border of the ectal facet, approximately at the confluence of the sustentaculum and the calcaneus body.
21	The intersection of the medial border of the ectal facet and the body of the calcaneus at the ectal facet distal terminus.
22	Midway between landmarks 15 and 21 on the distal border of the ectal facet.
23	The most plantar projecting point of the distal plantar tubercle.
24	The center of the plantar border of the heel.
25	The most proximally projecting point on the medial border of the heel.
26	The most dorsally projecting point on the dorsal border of the heel.
27	The most proximally projecting point on the lateral border of the heel.

APPENDIX: B

APPENDIX B. Description of Calcaneal Characters for Cladistic Analysis

Character number	Character name in matrix	Reference	Original states, if modified	New character states
224	Calcaneal width/ length	Modified from Patel et al. 2012, character 225	(0) <35; (1) Polymorphic, 0/2; (2) >35, <40; (3) polymorphic, 2/4; (4) >40, <45; (5) polymorphic, 4/6; (6) >45	(0) <35; (1) Polymorphic, 0/2; (2) >35, <40; (3) polymorphic, 2/4; (4) >40, <45; (5) polymorphic, 4/6; (6) >45,<50; (7) polymorphic, 6/8; (8) >50,<55; (9) polymorphic, 8/A; (A) >55
225	Distal calcaneal elongation (length of calcaneus distal to ectal facet/total calcaneal length x 100)	Modified from Patel et al., 2012, character 232 (which was modified from Dagosto, 1990, character 5)	(0) <40; (1) Polymorphic, 0/2; (2) >40, <45; (3) polymorphic, 2/4; (4) >45, <60; (5) polymorphic, 4/6; (6) >60	(0) >30,<40; (1) Polymorphic, 0/2; (2) >41,<50; (3) polymorphic, 2/4; (4) >51,<60; (5) polymorphic, 4/6; (6) >61,<70; (7) polymorphic, 6/8; (8) >71
226	Proximal calcaneal elongation (length from proximal border of ectal facet to proximal end of calcaneus/calcaneus length)	Modified from Gebo et al., 2001, character 10	(0) <25; (1) 25–30; (2) >30	(0) 0.10–0.15; (1) polymorphic, 0/2; (2) 0.16–0.20; (3) Polymorphic, 2/4; (4) 0.21–0.25; (5) polymorphic, 4/6; (6) 0.26–0.30; (7) polymorphic, 6/8; (8) >0.31
227	Relative length of ectal facet (ectal facet width/ectal facet length)	Same as Patel et al., 2012, character 226 (originally used by Gebo et al., 2001, their character 8)		(0) <50; (1) Polymorphic, 0/2; (2) >50, <60; (3) polymorphic, 2/4; (4) >60
228	Ectal facet radius of curvature	New character		(0) <120°; (1) ≥120°
229	Ectal facet flange development	New character		(0) Absent; (1) intermediate; (2) present
230	Bony distinction between plantar edge of ectal facet and body	New character		(0) No well-defined border; (1) well-defined border present
231	Size of calcaneal peroneal tubercle (100 × widest point on peroneal tubercle to ectal facet, measured perpendicular to long axis of bone/ calcaneal width)	Modified from Patel et al., 2012, character 228	(0) Massive, extends far laterally; (1) very small	(0) Massive, extends far laterally (≥21); (1) medium (<21); (2) highly reduced or too small to measure
232	Peroneal tubercle shape	New character		(0) Discrete tubercle with clearly defined borders; (1) tubercle gradually slopes into body (substantially longer proximodistally relative to mediolateral width)
233	Number of "peaks" on calcaneal peroneal tubercle	New character		(0) Single tubercle present; (1) two "peaks" present
234	Position of peroneal tubercle relative to sustentaculum	New character		(0) Proximal; (1) within proximal half of sustentaculum; (2) within distal half of sustentaculum

APPENDIX B . Continued

Character number	Character name in matrix	Reference	Original states, if modified	New character states
235	Position of the peroneal tubercle relative to the ectal facet	Modified from Patel et al., 2012, character 227 (Modified from Dagosto, 1988, character 10)	(0) Maximum width of peroneal tubercle is placed distal to distal terminus of ectal facet; (1) maximum width of peroneal tubercle is placed approximately at the distal terminus of the ectal facet; (2) maximum width of peroneal tubercle is placed proximal to the distal terminus of the ectal facet	(0) Maximum width of peroneal tubercle is placed distal to distal terminus of ectal facet; (1) maximum width of peroneal tubercle is placed approximately at the distal terminus of the ectal facet; (2) maximum width of peroneal tubercle is placed proximal to the distal terminus of the ectal facet, closer to the distal terminus of the ectal facet than the proximal; (3) maximum width of peroneal tubercle is placed proximal to distal terminus of the ectal facet, closer to the proximal terminus of the ectal facet than distal
236	Development of distal plantar tubercle on calcaneus	Same as Patel et al., 2012, character 229		(0) Small, poorly developed; (1) polymorphic, 0/2; (2) well-developed
237	Level of distal plantar tubercle (tubercle to cuboid facet/calcaneal length)	New character		(0) Distal, near cuboid facet (0–0.19); (1) more proximal (>0.20)
238	Orientation of long axis of calcaneocuboid joint	Same as Patel et al., 2012, character 230		(0) Dorsoventral; (1) oblique; (2) mediolateral;
239	Calcaneocuboid joint shape	Modified from Patel et al., 2012, character 231 (Modified from Gebo et al., 2001, character 11)	(0) Oval; (1) fan-shaped, notch is articular; (2) fan-shaped, notch is nonarticular	(0) Oval; (1) fan-shaped, notch is articular; (2) fan-shaped, notch is nonarticular; (3) oval but longest in dorsoplantar direction
240	Concavity of cuboid facet	Modified from Ford, 1980, 1986, character 10	(0) Flat cuboid articular surface; (1) slightly concave (or cuboid pivot or convex latero-plantarly); (2) moderately concave; (3) deeply concave	(0) Flat (≥160); (1) shallow (≥150, <160); (2) deep (<150)
241	Dorsal extension of bone supporting cuboid facet	New character		(0) Absent; (1) present
242	Posterior (plantar) calcaneal bowing	Modified from Patel et al., 2012, character 23(3) (Modified from Dagosto and Gebo, 1994, character C3)	(0) Absent; (1) present	(0) Absent; (1) present, moderately developed; (2) present, extreme bowing
243	Mediolateral bowing of calcaneal tuber	New character		(0) Absent; (1) present, moderate bowing; (2) present, extreme bowing

APPENDIX B . Continued

Character number	Character name in matrix	Reference	Original states, if modified	New character states
244	Calcaneal sustentacular facet configuration	Same as Patel et al., 2012, character 234		(0) Single continuous sustentacular facet present; (1) polymorphic, 0/2; (2) separate anterior and posterior sustentacular facets present
245	Form of medial margin between sustentaculum and distal sustentacular facet (viewed dorsally)	Modified from Ford, 1980, 1986, character 5	(0) Medial edge of sustentaculum astragali straight, no waisting; (1) waisted; (2) split distribution; some individuals with straight medial edge; (3) secondary loss of waisting; all with straight edge	(0) Waisted into body; (1) relatively linear medial margin
246	Facet distal to the distal extension of the sustentacular facet (navicular or otherwise)	Modified from Ford, 1980, 1986, character 19	(0) No navicular articular surface; (1) split distribution; some individuals with facet; (2) facet anterior (distal) to anterior)	(0) Prominent; (1) very small or absent
247	Angle between sustentaculum and ectal facet	New character		(0) <140; (1) >140–<160; (2) >160–<180; (3) >180
248	Shape of medial edge of sustentaculum in plantar view	New character		(0) Triangular or beak-like; (1) rounded
249	Morphology of groove for flexor fibularis under sustentaculum	Modified from Ford, 1980, 1986, character 24	(0) Sulcus shallow; (1) moderately deep; (2) deep	(0) No noticeable groove present; (1) deep medially with distinct groove or wall
250	Position of distal terminus of ectal facet relative to anterior calcaneal segment	New character		(0) Dorsally positioned on body; (1) intermediate condition; (2) sunk into body plantarly
251	Size of tuber calcanei	Modified from Ford, 1980, 1986, character 26	(0) Tuber calcanei small and indistinct; (1) moderately large tubercle in some specimens; (2) very large tubercle	(0) Relatively small (sliver, oval, no clear insertion for tendo calcanei); (1) medium (large in one direction, insertion for tendo calcanei present but not robust); (2) relatively large
252	Shape of tuber calcanei	New character		(0) Oval; (1) square/rectangular; (2) uneven walls/trapezoidal; (3) proximally projecting medial wall
253	Dorsal heel process	New character		(0) Tucked under ectal facet in lateral view; (1) level with ectal facet in lateral view; (2) projects dorsal to ectal facet

APPENDIX: C

APPENDIX C. Character Matrix of Calcaneal Characters (Add "223" to "Character Numbers" Below to Match Scores with Characters in Appendix C)

Character number	1 1234567890	2 1234567890	3 1234567890
Absarokius sp.	2442020010	1021101000	1001011110
Adapis parisiensis	3084011200	0320101011	1011111120
Aegyptopithecus zeuxis	???4011010	020?1220??	2011012???
Allenopithecus nigroviridis	9084001000	1101121000	0001012222
Alouatta seniculus	8062111010	0200122000	0111112211
Aotus trivirgatus	6084121010	1100121000	0001011211
Apidium phiomense	8084000010	2021220000	2001001110
Arapahovius gazini	2424020110	2021101000	0000000110
Arctocebus calabarensis	5244020--1	--00022022	0113100000
Asiadapis cambayensis	806202?000	1221102000	0001101?0
Cantius abditus	5260000100	1000201000	1000100110
Carpolestes simpsoni	A064021000	2000230000	0111101100
Cheirogaleus major	2242121210	0220112001	0001100130
Darwinius masillae	?2???????0	?10???????	??0???????
Eosimias sinensis	5262001110	1001221000	10?0101100
Europolemur klatti	22?0???010	?20?1???0?	?0??1?1???
Galago moholi	0823020100	0220112101	2002110231
Galagoides demidoff	0802020110	1100112101	2002110230
Hemiacodon gracilis	0260000110	1121201000	0001111000
Komba spp.	0444000210	0320112001	2001100230
Lemur catta	3283000200	0220111000	0002100221
Lepilemur mustelinus	2362020110	1200121001	0003102122
Leptadapis magnus	5062000100	0321112011	0112100120
Loris tardigradus	5222120--1	--21022022	0103100000
Marcgodinotius indicus	5060100000	1001101010	0010101000
Microcebus murinus	0622000210	1120110000	0111100130
Microchoerus erinaceus	???2010210	2???????00	???1100???
Nannopithex abderhaldeni	???4???1??	???2???????	??????????
Necrolemur spp.	0600010200	02??????00	00?1101211
Nycticebus coucang	6083110--1	--20022022	0113100000
Omomys sp.	0464021110	1121101000	0001111211
Otolemur crassicaudatus	0622020100	0220112101	2002100230
Pan troglodytes	A084121000	1201121000	0112011210
Perodicticus potto	7064010--1	--21022022	0113100000
Plesiadapis tricuspidens	A082010000	2000230000	0110001100
Propithecus spp.	2060000200	0320100001	0003111222
Propliopithecus chirobates	???20?0?1?	??0?12????	00?1012???
Proteopithecus sylviae	6284000010	2021121000	2000011111
Saimiri sciureus	7264121010	1120121001	0001012211
Shoshonius cooperi	0442011110	1121101000	?00?100000
Tarsius bancanus	0802021200	0320100000	2011101231
Teilhardina belgica	1442000010	2021200000	0001100000
Tetonius sp.	2443021010	2021??1000	100101?110
Tupaia spp.	A084021010	1000130000	0010001110
Varecia variegata	2260000200	0300111001	0002101222
Washakius insignis	0442020100	2121101000	0002010110

LITERATURE CITED

Bajpai S, Kay RF, Williams BA, Das DP, Kapur VV, Tiwari BN. 2008. The oldest Asian record of Anthropoidea. Proc Natl Acad Sci USA 105:11093–11098.

Beard KC, Marivaux L, Tun ST, Soe AN, Chaimanee Y, Htoon W, Marandat B, Aung HH, Jaeger J-J. 2007. New sivaladapid primates from the Eocene Pondaung Formation of Myanmar and the anthropoid status of Amphipithecidae. Bull Carnegie Mus Nat Hist 39:67–76.

Beard KC, Qi T, Dawson MR, Wang B, Li C. 1994. A diverse new primate fauna from middle Eocene fissure-fillings in southeastern China. Nature 368:604–609.

Bookstein FL. 1991. Morphometric tools for landmark data. New York: Cambridge University Press.

Bown TM, Kraus MJ. 1988. Geology and paleoenvironment of the Oligocene Jebel Qatrani Formation and adjacent rocks, Fayum Depression, Egypt. US Geol Surv Prof Paper 1452:1–64.

Boyer DM, Seiffert ER, Simons EL. 2010. Astragalar morphology of *Afradapis*, a large adapiform primate from the earliest late Eocene of Egypt. Am J Phys Anthropol 143:383–402.

Chaimanee Y, Chavasseau O, Beard KC, Kyaw AA, Soe AN, Sein C, Lazzari V, Marivaux L, Marandat B, Swe M, Rugbumrung M, Lwin T, Valentin X, Thein ZMM, Jaeger JJ. 2012. Late Middle Eocene primate from Myanmar and the initial anthropoid colonization of Africa. Proc Natl Acad Sci USA 109:10293–10297.

Conroy G. 1974. Primate postcranial remains from the Fayum Province, Egypt, U.A.R. Ph.D. Dissertation. New Haven, CT: Yale University.
Cooke SB, Tallman M. 2012. New endemic platyrrhine femur from Haiti: description and locomotor analysis. J Hum Evol 63:560–567.
Dagosto M, Gebo DL. 1994. Postcranial anatomy and the origin of the Anthropoidea. In: Fleagle JG, Kay RF, editors. Anthropoid origins. New York: Plenum Press. p 567–593.
Dagosto M. 1988. Implications of postcranial evidence for the origin of euprimates. J Hum Evol 17:35–56.
Dagosto M. 1990. Models for the origin of the anthropoid postcranium. J Hum Evol 19:121–139.
Drapeau MSM. 2008. Articular morphology of the proximal ulna in extant and fossil hominoids and hominins. J Hum Evol 55:86–102.
Fleagle J. 1983. Locomotor adaptations of Oligocene and Miocene hominoids and their phyletic implications. In: Ciochon RL, Corruccini RS, editors. New interpretations of ape and human ancestry. New York: Plenum Press. p 301–324.
Fleagle J, Simons E. 1982. Skeletal remains of *Propliopithecus chirobates* from the Egyptian Oligocene. Folia Primatol 39:161–177.
Fleagle J, Simons E, Conroy G. 1975. Ape limb bone from the Oligocene of Egypt. Science 189:135–137.
Ford SM. 1980. A systematic revision of the Platyrrhini based on features of the postcranium. Ph.D. Dissertation. Pittsburgh: University of Pittsburgh.
Ford SM. 1986. Systematics of the New World monkeys. In: Swindler DR, Erwin J, editors. Comparative primate biology, Vol. 1: Systematics, evolution, and anatomy. New York: Alan R. Liss. p 73–135.
Ford SM. 1988. Postcranial adaptations of the earliest platyrrhine. J Hum Evol 17:155–192.
Ford SM. 1994. Primitive platyrrhines. Perspectives on anthropoid origins from platyrrhine, parapithecid, and preanthropoid postcrania. In: Fleagle JG, Kay RF, editors. Anthropoid origins. New York: Plenum Press. p 595–673.
Gebo DL. 1986. Anthropoid origins–the foot evidence. J Hum Evol 15:421–430.
Gebo DL. 1988. Foot morphology and locomotor adaptation in Eocene primates. Folia Primatol 50:3–41.
Gebo DL. 1989. Locomotor and phylogenetic considerations in anthropoid evolution. J Hum Evol 18:201–233.
Gebo DL, Simons EL. 1987. Morphology and locomotor adaptations of the foot in early Oligocene anthropoids. Am J Phys Anthropol 74:83–101.
Gebo DL, Dagosto M, Beard KC, Ni X. 2008. New primate hind limb elements from the middle Eocene of China. J Hum Evol 55:999–1014.
Gebo D, Dagosto M, Beard KC, Qi T, Wang J. 2000. The oldest known anthropoid postcranial fossils and the early evolution of higher primates. Nature 404:276–278.
Gebo DL, Dagosto M, Beard KC, Qi T. 2001. Middle Eocene primate tarsals from China: implications for haplorhine evolution. Am J Phys Anthropol 116:83–107.
Gebo DL, Simons EL, Rasmussen D, Dagosto M. 1994. Eocene anthropoid postcrania from the Fayum, Egypt. In: Fleagle JG, Kay RF, editors. Anthropoid origins. New York: Plenum Press. p 203–233.
Gilbert CC. 2011. Phylogenetic analysis of the African papionin basicranium using 3-D geometric morphometrics: the need for improved methods to account for allometric effects. Am J Phys Anthropol 144:60–71.
Gower JC. 1975. Generalized Procrustes analysis. Psychometrika 40:33–55.
Halenar LB. 2011. Reconstructing the locomotor repertoire of *Protopithecus brasiliensis*. II. Forelimb morphology. Anat Rec 294:2048–2063.
Hammer Ø, Harper DAT, Ryan PD. 2001. PAST: Paleontological Statistics Software Package for Education and Data Analysis. Paleontol Electron 4:9 pp. Accessed December 2010, http://palaeo-electronica.org/2001_1/past/issue1_01.htm.
Hammer Ø, Harper DAT. 2006. Paleontological data analysis. Oxford: Blackwell Publishing.
Harcourt-Smith WEH, Tallman M, Frost SR, Wiley DF, Rohlf FJ, Delson E. 2008. Analysis of selected hominoid joint surfaces using laser scanning and geometric morphometrics: a preliminary report. In: Sargis EJ, Dagosto M, editors. Mammalian evolutionary morphology: a tribute to Frederick S. Szalay. Dordrecht: Springer. p 373–383.
Harmon EH. 2007. The shape of the hominoid proximal femur: a geometric morphometric analysis. J Anat 210:170–185.
Harmon EH. 2009. Size and shape variation in the proximal femur of *Australopithecus africanus*. J Hum Evol 56:551–559.
Holliday TW, Hutchinson VT, Morrow MMB, Livesay GA. 2010. Geometric morphometric analyses of hominid proximal femora: taxonomic and phylogenetic considerations. HOMO 61:3–15.
Jaeger JJ, Thein T, Benammi M, Chaimanee Y, Soe AN, Lwin T, Tun T, Wai S, Ducrocq S. 1999. A new primate from the Middle Eocene of Myanmar and the Asian early origin of anthropoids. Science 286:528–530.
Kay R. 2012. Evidence for an Asian origin of stem anthropoids. Proc Natl Acad Sci USA 109:10132–10133.
Kay RF, Williams BA, Ross CF, Takai M, Shijehara N. 2004. Anthropoid origins: a phylogenetic analysis. In: Ross CF, Kay RF, editors. Anthropoid origins: new visions. New York: Kluwer Academic/Plenum Publishers. p 91–135.
Langdon JH. 1986. Functional morphology of the Miocene hominoid foot. Contrib Primatol 22:1–225.
Lockwood CA, Kimbel WH, Lynch JM. 2004. Morphometrics and hominoid phylogeny: support for a chimpanzee–human clade and differentiation among great ape subspecies. Proc Natl Acad Sci USA 101:4356–4360.
Marivaux L. 2006. The eosimiid and amphipithecid primates (Anthropoidea) from the Oligocene of the Bugti Hills (Balochistan, Pakistan): new insight into early higher primate evolution in South Asia. Paleovertebrata 34:29–109.
Marivaux L, Antoine PO, Baqri SRH, Benammi M, Chaimanee Y, Crochet JY, De Franceschi D, Iqbal N, Jaeger JJ, Métais G, Roohi G, Welcomme J-L. 2005. Anthropoid primates from the Oligocene of Pakistan (Bugti Hills): data on early anthropoid evolution and biogeography. Proc Natl Acad Sci USA 102:8436–8441.
Miller ER, Simons EL. 1997. Dentition of *Proteopithecus sylviae*, an archaic anthropoid from the Fayum, Egypt. Proc Natl Acad Sci USA 94:13760–13764.
Moyà-Solà S, Köhler M, Alba DM, Roig I. 2012. Calcaneal proportions in primates and locomotor inferences in *Anchomomys* and other Paleogene Euprimates. Swiss J Paleontol 131:147–159.
O'Higgins P, Jones N. 2006. Tools for statistical shape analysis. Hull York Medical School. Accessed December 2010, http://sites.google.com/site/hymsfme/resources.
Patel BA, Seiffert ER, Boyer DM, Jacobs RL, St. Clair EM, Simons EL. 2012. New primate first metatarsals from the Paleogene of Egypt and the origin of the anthropoid big toe. J Hum Evol 63:99–120.
Perelman P, Johnson WE, Roos C, Seuánez HN, Horvath JE, Moreira MAM, Kessing B, Pontius J, Roelke M, Rumpler Y, Schneider MPC, Silva A, O'Brien SJ, Pecon-Slattery J. 2011. A molecular phylogeny of living primates. PLoS Genet 7:e1001342.
Rohlf FJ, Slice D. 1990. Extensions of the Procrustes method for the optimal superimposition of landmarks. Syst Biol 39:40–59.
Rose KD, Rana RS, Sahni A, Kumar K, Missiaen P, Singh L, Smith T. 2009. Early Eocene primates from Gujarat, India. J Hum Evol 56:366–404.
Rose M. 1994. Quadrupedalism in some Miocene catarrhines. J Hum Evol 26:387–411.
Rose M. 1997. Phylogenetic features of the forelimb in Miocene hominoids. In: Begun DR, Ward CV, Rose MD, editors. Function, phylogeny, and fossils: Miocene hominoid evolution and adaptations. New York: Plenum Press. p 79–100.
Ross C, Williams B, Kay RF. 1998. Phylogenetic analysis of anthropoid relationships. J Hum Evol 35:221–306.
Ryan TM, Silcox MT, Walker A, Mao X, Begun DR, Benefit BR, Gingerich PD, Köhler M, Kordos L, McCrossin ML, Moyà-Solà S, Sanders WJ, Seiffert ER, Simons E, Zalmout IS,

Spoor F. 2012. Evolution of locomotion in Anthropoidea: the semicircular canal evidence. Proc R Soc B 279:3467–3475.
Sarmiento EE. 1983. The significance of the heel process in anthropoids. Int J Primatol 4:127–152.
Seiffert ER. 2006. Revised age estimates for the later Paleogene mammal faunas of Egypt and Oman. Proc Natl Acad Sci USA 103:5000–5005.
Seiffert ER. 2012. Early primate evolution in Afro-Arabia. Evol Anthropol 21:239–253.
Seiffert ER, Perry JMG, Simons EL, Boyer DM. 2009. Convergent evolution of anthropoid-like adaptations in Eocene adapiform primates. Nature 461:1118–1121.
Seiffert ER, Simons EL. 2001. Astragalar morphology of late Eocene anthropoids from the Fayum Depression (Egypt) and the origin of catarrhine primates. J Hum Evol 41:577–606.
Seiffert ER, Simons EL, Boyer DM, Perry JMG, Ryan TM, Sallam HM. 2010a. A fossil primate of uncertain affinities from the earliest late Eocene of Egypt. Proc Natl Acad Sci USA 107:9712–9717.
Seiffert ER, Simons EL, Clyde WC, Rossie JB, Attia Y, Bown TM, Chatrath P, Mathison ME. 2005a. Basal anthropoids from Egypt and the antiquity of Africa's higher primate radiation. Science 310:300–304.
Seiffert ER, Simons EL, Fleagle JG. 2000. Anthropoid humeri from the late Eocene of Egypt. Proc Natl Acad Sci USA 97:10062–10067.
Seiffert ER, Simons EL, Fleagle JG, Godinot M. 2010b. Paleogene anthropoids. In: Werdelin L, Sanders WJ, editors. Cenozoic mammals of Africa, 1st ed. Berkeley: University of California Press. p 369–391.
Seiffert ER, Simons EL, Ryan TM, Attia Y. 2005b. Additional remains of *Wadilemur elegans*, a primitive stem galagid from the late Eocene of Egypt. Proc Natl Acad Sci USA 102:11396–11401.
Seiffert ER, Simons EL, Simons CVM. 2004. Phylogenetic, biogeographic, and adaptive implications of new fossil evidence bearing on crown anthropoid origins and early stem catarrhine evolution. In: Ross CF, Kay RF, editors. Anthropoid origins: new visions. New York: Kluwer Academic/Plenum Publishers. p 157–181.
Simons EL. 1989. Description of two genera and species of Late Eocene Anthropoidea from Egypt. Proc Natl Acad Sci USA 86:9956–9960.
Simons EL. 1997. Preliminary description of the cranium of *Proteopithecus sylviae*, an Egyptian late Eocene anthropoidean primate. Proc Natl Acad Sci USA 94:14970–14975.
Simons EL, Seiffert ER. 1999. A partial skeleton of *Proteopithecus sylviae* (Primates, Anthropoidea): first associated dental and postcranial remains of an Eocene anthropoidean. Comptes Rendus de l'Académie des Sciences-Series IIA-Earth and Planetary Science 329:921–927.
Steiper ME, Seiffert ER. 2012. Evidence for a convergent slowdown in primate molecular rates and its implications for the timing of early primate evolution. Proc Natl Acad Sci USA 109:6006–6011.
Strasser E. 1988. Pedal evidence for the origin and diversification of cercopithecid clades. J Hum Evol 17:225–245.
Swofford DL. 2002. PAUP*: Phylogenetic Analysis Using Parsimony (*and Other Methods), version 4. Sunderland, MA: Sinauer Associates.
Szalay FS, Decker RL. 1974. Origins, evolution and function of the tarsus in late Cretaceous eutheria and Paleocene primates. In: Jenkins FA, editor. Primate locomotion. New York: Academic Press. p 223–259.
Takai M, Anaya F, Shigehara N, Setoguchi T. 2000. New fossil materials of the earliest New World monkey, *Branisella boliviana*, and the problem of platyrrhine origins. Am J Phys Anthropol 111:263–281.
Tallman M. 2012. Morphology of the distal radius in extant hominoids and fossil hominins: Implications for the evolution of bipedalism. Anat Rec 295:454–464.
Wiley DF, Amenta N, Alcantara DA, Ghosh D, Kil YJ, Delson E, Harcourt-Smith W, Rohlf FJ, St John K, and Hamann B. 2005. Evolutionary morphing. Visualization VIS 05. IEEE:431–438.
Young NM. 2008. A comparison of the ontogeny of shape variation in the anthropoid scapula: functional and phylogenetic signal. Am J Phys Anthropol 136:247–264.